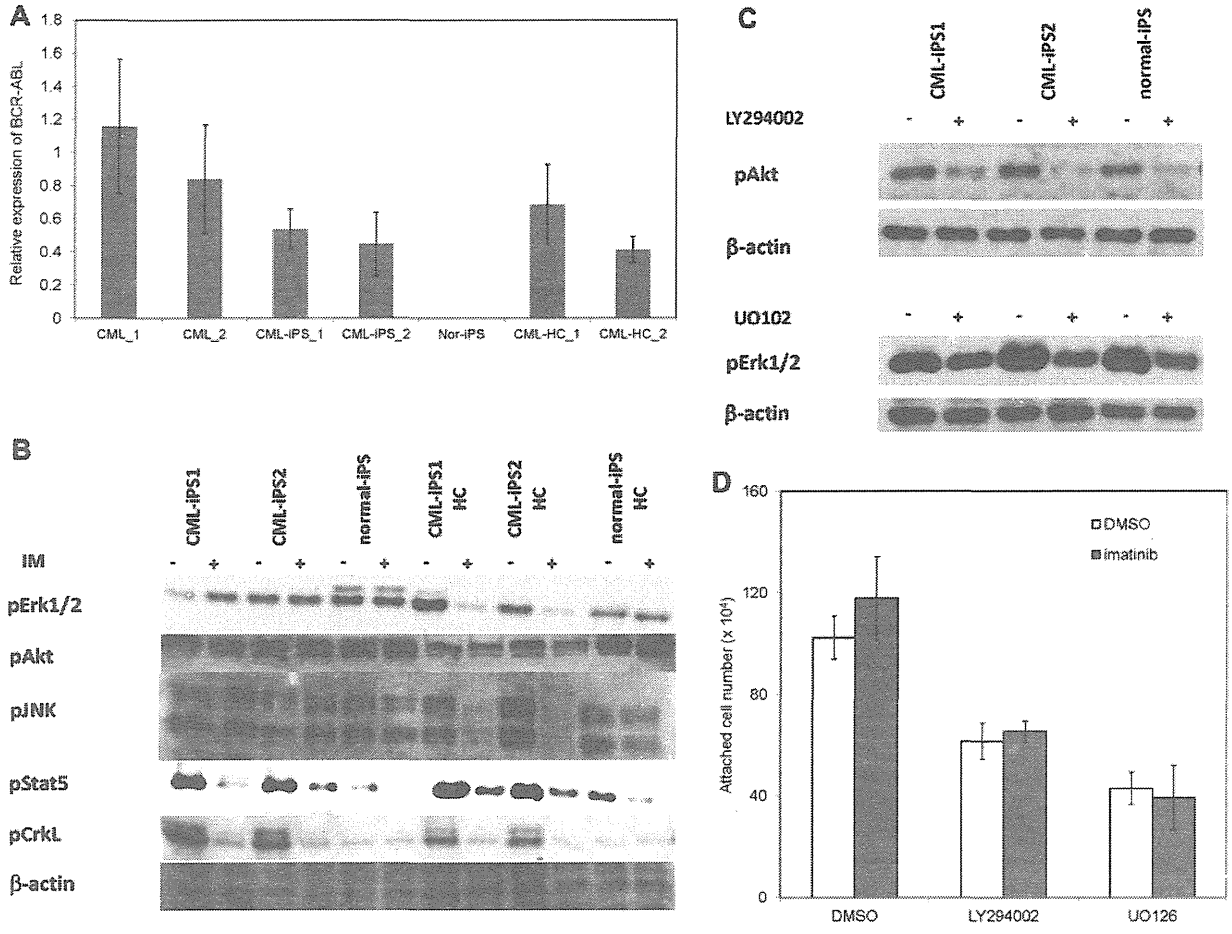

Figure 6. The mechanism of imatinib resistance in the CML-iPSCs. (A) The expression profile of BCR-ABL transcript during hematopoietic differentiation. The expression levels of BCR-ABL in the CML-iPSCs were compared with those of primary CML samples (CML_1 and CML_2), CML-iPSC–derived CD34$^+$ hematopoietic cells (CML-HC_1 and CML-HC_2), and normal iPSC (nor-iPS). The expression level of the mean in the primary CML sample was set at 1. (B) BCR-ABL signaling was estimated in the CML-iPSCs after imatinib (IM) treatment. The phosphorylation state of ERK1/2, AKT, JNK, and STAT5, which are the essential for the survival of BCR-ABL (+) hematopoietic progenitors (CD34$^+$CD45$^+$), were evaluated after imatinib treatment in CML-iPSCs. These were the representative data from 3 independent experiments. (C-D) LY294002 and U0126 (10μM) were added to the culture of CML iPSCs to inhibit AKT and ERK, respectively with or without imatinib. (C) After 4 hours of culture, each inhibitor decreased the phosphorylation of ERK or AKT as expected. (D) The attached cell numbers after treatment with specific AKT or ERK inhibitor were shown. These were the representative data from 3 independent experiments.

The progression of CML from initial indolent CP to the aggressive stages, the AP and BC is caused by additional gene mutations. If we introduce some additional mutation into the CML-iPSCs, the CML BC model may be generated.

Generation of hematologic malignancies derived iPSCs other than CML

Primary samples of hematologic malignancy are usually difficult to be expanded. However, after they are reprogrammed to iPSCs, they can expand unlimitedly. As a result, we can obtain the genetically abnormal hematopoietic cells continuously by redifferentiating them into hematopoietic cells and use them for the studies which require the large number of living cells, such as the analysis for proteome, epigenome, transciptome, leukemia stem cells, or drug screening. Thus, iPSCs technology would be useful for the study of hematologic malignancy based on the patient samples.

However, reprogramming of leukemia cells may be harder than generation of normal iPSCs because of the genetic and epigenetic status of leukemia cells. To overcome the difficulty, application of other factors in addition to the Yamanaka factors may be effective, such as exogenous expression of miRNA-302,[48] chemical compounds, such as azacitidine (DNA metyltranferase inhibitor),[49] BIX01294 (G9a histone metyltransferase inhibitor),[50] VPA (histone deacetylase inhibitor), or TSA (histone deacetylase inhibitor),[26] and knockdown of p53, p21, and Ink4/Arf.[51,52]

In addition, there may be more desirable gene delivery system for iPSC generation for the study of disease pathogenesis. The integration site of retrovirus in the iPSCs may affect the gene expression and change the disease phenotype after redifferentiating them into the original lineages. Recently, efficient induction of transgene free iPSCs, such as using Sendai virus system, was reported[53] and will be applicable for the disease derived iPSCs. We could establish the CML-iPSCs by this system. Using the newly established CML-iPSCs with sendai virus and feeder free culture system, we confirmed the same resistance to imatinib (supplemental Figure 4). Furthermore, without feeder cells, the phosphorylation of ERK and AKT were maintained, although the phosphorylation of STAT5 and CRKL were decreased by imatinib treatment.

In addition, the sendai virus system can be applied to the establishment of other disease derived iPSCs.

Acknowledgments

The authors thank T. Kitamura for pMXs retroviral vector; and Y. Hokama, M. Kobayashi, and Y. Oikawa for expert technical assistance.

This work was supported in part by a Grant-in-Aid for Scientific Research from the Japan Society for the Promotion of Science and by Health and Labor Sciences Research grants from the Ministry of Health, Labor and Welfare, Japan and a grant-in-aid from Core Research for Evolutional Science and Technology of Japan.

Authorship

Contribution: K.K. designed the research, performed experiments, and wrote the paper; S.A., M.H., K.T., N.T., M.O., G.N., K.U., K.N., and Y.K. performed experiments, K.E., H.A., and H.N. discussed the paper; and M.K. conceived and designed the research, supervised the whole project, and wrote the paper.

Conflict-of-interest disclosure: The authors declare no competing financial interests.

Correspondence: Mineo Kurokawa, Deptartment of Hematology and Oncology, Graduate School of Medicine, University of Tokyo, 7-3-1 Hongo, Bunkyo-ku, Tokyo 113-8655, Japan; e-mail: kurokawa-tky@umin.ac.jp.

References

1. Giles FJ, Keating A, Goldstone AH, Avivi I, Willman CL, Kantarjian HM. Acute myeloid leukemia. *Hematology.* 2002;2002(1):73-110.
2. Haferlach T. Molecular genetic pathways as *therapeutic targets in acute myeloid leukemia. Hematology.* 2008;2008(1):400-411.
3. Barabé F, Kennedy JA, Hope KJ, Dick JE. Modeling the initiation and progression of human acute leukemia in mice. *Science.* 2007;316(5824):600-604.
4. Takahashi K, Yamanaka S. Induction of pluripotent stem cells from mouse embryonic and adult fibroblast cultures by defined factors. *Cell.* 2006; 126(4):663-676.
5. Wernig M, Meissner A, Foreman R, et al. In vitro reprogramming of fibroblasts into a pluripotent ES-cell-like state. *Nature.* 2007;448(7151):318-324.
6. Okita K, Ichisaka T, Yamanaka S. Generation of germline-competent induced pluripotent stem cells. *Nature.* 2007;448(7151):313-317.
7. Meissner A, Wernig M, Jaenisch R. Direct reprogramming of genetically unmodified fibroblasts into pluripotent stem cells. *Nat Biotechnol.* 2007; 25(10):1177-1181.
8. Yu J, Vodyanik MA, Smuga-Otto K, et al. Induced pluripotent stem cell lines derived from human somatic cells. *Science.* 2007;318(5858):1917-1920.
9. Takahashi K, Tanabe K, Ohnuki M, et al. Induction of pluripotent stem cells from adult human fibroblasts by defined factors. *Cell.* 2007;131(5): 861-872.
10. Park I-H, Zhao R, West JA, et al. Reprogramming of human somatic cells to pluripotency with defined factors. *Nature.* 2008;451(7175):141-146.
11. Nishikawa S, Goldstein RA, Nierras CR. The promise of human induced pluripotent stem cells for research and therapy. *Nat Rev Mol Cell Biol.* 2008;9(9):725-729.
12. Park I-H, Arora N, Huo H, et al. Disease-specific induced pluripotent stem cells. *Cell.* 2008;134(5): 877-886.
13. Hanna J, Wernig M, Markoulaki S, et al. Treatment of sickle cell anemia mouse model with iPS cells generated from autologous skin. *Science.* 2007;318(5858):1920-1923.
14. Yamanaka S. Strategies and new developments in the generation of patient-specific pluripotent stem cells. *Cell Stem Cell.* 2007;1(1):39-49.
15. Ye L, Chang JC, Lin C, Sun X, Yu J, Kan YW. Induced pluripotent stem cells offer new approach to therapy in thalassemia and sickle cell anemia and option in prenatal diagnosis in genetic diseases. *Proc Natl Acad Sci U S A.* 2009;106(24): 9826-9830.
16. Raya A, Rodriguez-Piza I, Guenechea G, et al. Disease-corrected haematopoietic progenitors from Fanconi anaemia induced pluripotent stem cells. *Nature.* 2009;460(7251):53-59.
17. Carette JE, Pruszak J, Varadarajan M, et al. Generation of iPSCs from cultured human malignant cells. *Blood.* 2010;115(20):4039-4042.
18. Miyoshi N, Ishii H, Nagai K-i, et al. Defined factors induce reprogramming of gastrointestinal cancer cells. *Proc Natl Acad Sci U S A.* 2010;107(1):40-45.
19. Utikal J, Maherali N, Kulalert W, Hochedlinger K. Sox2 is dispensable for the reprogramming of melanocytes and melanoma cells into induced pluripotent stem cells. *J Cell Sci.* 2009;122(19): 3502-3510.
20. Ye Z, Zhan H, Mali P, et al. Human-induced pluripotent stem cells from blood cells of healthy donors and patients with acquired blood disorders. *Blood.* 2009;114(27):5473-5480.
21. Sawyers CL. Chronic myeloid leukemia. *New Engl J Med.* 1999;340(17):1330-1340.
22. Takayama N, Nishimura S, Nakamura S, et al. Transient activation of c-MYC expression is critical for efficient platelet generation from human induced pluripotent stem cells. *J Exp Med.* 2010; 207(13):2817-2830.
23. Hayashi Y, Chan T, Warashina M, et al. Reduction of N-glycolylneuraminic acid in human induced pluripotent stem cells generated or cultured under feeder and serum-free defined conditions. *PLoS One.* 2010;5(11):e14099.
24. Takayama N, Nishikii H, Usui J, et al. Generation of functional platelets from human embryonic stem cells in vitro via ES-sacs, VEGF-promoted structures that concentrate hematopoietic progenitors. *Blood.* 2008;111(11):5298-5306.
25. Okabe M, Otsu M, Ahn DH, et al. Definitive proof for direct reprogramming of hematopoietic cells to pluripotency. *Blood.* 2009;114(9):1764-1767.
26. Huangfu D, Osafune K, Maehr R, et al. Induction of pluripotent stem cells from primary human fibroblasts with only Oct4 and Sox2. *Nat Biotechnol.* 2008;26(11):1269-1275.
27. Chan EM, Ratanasirintrawoot S, Park I-H, et al. Live cell imaging distinguishes bona fide human iPS cells from partially reprogrammed cells. *Nat Biotechnol.* 2009;27(11):1033-1037.
28. Nagae G, Isagawa T, Shiraki N, et al. Tissue-specific demethylation in CpG-poor promoters during cellular differentiation. *Hum Mol Genet.* 2011;20(14):2710-2721.
29. Goyama S, Yamamoto G, Shimabe M, et al. Evi-1 is a critical regulator for hematopoietic stem cells and transformed leukemic cells. *Cell Stem Cell.* 2008;3(2):207-220.
30. Gutiérrez MI, Timson G, Siraj AK, et al. Single monochrome real-time RT-PCR assay for identification, quantification, and breakpoint cluster region determination of t(9;22) transcripts. *J Mol Diagn.* 2005;7(1):40-47.
31. Nishino K, Toyoda M, Yamazaki-Inoue M, et al. DNA methylation dynamics in human induced *pluripotent stem cells over time. PLoS Genet.* 2011;7(5):e1002085.
32. Ishikawa F, Yoshida S, Saito Y, et al. Chemotherapy-resistant human AML stem cells home to and engraft within the bone-marrow endosteal region. *Nat Biotechnol.* 2007;25(11): 1315-1321.
33. O'Brien SG, Guilhot F, Larson RA, et al. Imatinib compared with interferon and low-dose cytarabine for newly diagnosed chronic-phase chronic myeloid leukemia. *New Engl J Med.* 2003; 348(11):994-1004.
34. Druker BJ. Circumventing resistance to kinase-*inhibitor therapy. New Engl J Med.* 2006;354(24): 2594-2596.
35. Jiang X, Zhao Y, Smith C, et al. Chronic myeloid leukemia stem cells possess multiple unique features of resistance to BCR-ABL targeted therapies. *Leukemia.* 2007;21(5):926-935.
36. Steelman LS, Pohnert SC, Shelton JG, Franklin RA, Bertrand FE, McCubrey JA. JAK//STAT, Raf//MEK//ERK, PI3K//Akt and BCR-ABL in cell cycle progression and leukemogenesis. *Leukemia.* 2004;18(2):189-218.
37. Raitano AB, Halpern JR, Hambuch TM, Sawyers CL. The Bcr-Abl leukemia oncogene activates Jun kinase and requires Jun for transformation. *Proc Natl Acad Sci U S A.* 1995; 92(25):11746-11750.
38. Nichols GL, Raines MA, Vera JC, Lacomis L, Tempst P, Golde DW. Identification of CRKL as the constitutively phosphorylated 39-kD tyrosine phosphoprotein in chronic myelogenous leukemia cells. *Blood.* 1994;84(9):2912-2918.
39. Wang X, Lin G, Martins-Taylor K, Zeng H, Xu R-H. Inhibition of caspase-mediated anoikis is critical for basic fibroblast growth factor-sustained culture of human pluripotent stem cells. *J Biol Chem.* 2009;284(49):34054-34064.
40. Brill LM, Xiong W, Lee K-B, et al. Phosphoproteomic analysis of human embryonic stem cells. *Cell Stem Cell.* 2009;5(2):204-213.
41. Mahon F, Delphine R, Guilhot JL, et al. Discon*tinuation of imatinib in patients with chronic my*eloid leukaemia who have maintained complete molecular remission for at least 2 years: the prospective, multicentre stop imatinib (STIM) trial. *Lancet Oncol.* 2010;11(11):1029-1035.
42. Corbin AS, Agarwal A, Loriaux M, Cortes J, Deininger MW, Druker BJ. Human chronic myeloid leukemia stem cells are insensitive to imatinib despite inhibition of BCR-ABL activity. *J Clin Invest.* 2011;121(1):396-409.
43. Hamilton A, Helgason GV, Schemionek M, et al.

Chronic myeloid leukemia stem cells are not dependent on Bcr-Abl kinase activity for their survival. *Blood.* 2012;119(6):1501-1510.

44. Sloma I, Jiang X, Eaves AC, Eaves CJ. Insights into the stem cells of chronic myeloid leukemia. *Leukemia.* 2010;24(11):1823-1833.
45. Zhao C, Blum J, Chen A, et al. Loss of beta-catenin impairs the renewal of normal and CML stem cells in vivo. *Cancer Cell.* 2007;12(6):528-541.
46. Ding VMY, Ling L, Natarajan S, Yap MGS, Cool SM, Choo ABH. FGF-2 modulates Wnt signaling in undifferentiated hESC and iPS cells through activated PI3-K/GSK3beta signaling. *J Cell Physiol.* 2010;225(2):417-428.
47. Hu K, Yu J, Suknuntha K, et al. Efficient generation of transgene-free induced pluripotent stem cells from normal and neoplastic bone marrow and cord blood mononuclear cells. *Blood.* 2011; 117(14):e109-e119.
48. Lin S-L, Chang DC, Lin C-H, Ying S-Y, Leu D, Wu DTS. Regulation of somatic cell reprogramming through inducible mir-302 expression. *Nucleic Acids Res.* 2011;39(3):1054-1065.
49. Han J, Sachdev PS, Sidhu KS. A combined epigenetic and non-genetic approach for reprogramming human somatic cells. *PLoS One.* 2010;5(8): e12297.
50. Plews JR, Li J, Jones M, et al. Activation of pluripotency genes in human fibroblast cells by a novel mRNA based approach. *PLoS One.* 2010; 5(12):e14397.
51. Li H, Collado M, Villasante A, et al. The Ink4/Arf locus is a barrier for iPS cell reprogramming. *Nature.* 2009;460(7259):1136-1139.
52. Utikal J, Polo JM, Stadtfeld M, et al. Immortalization eliminates a roadblock during cellular reprogramming into iPS cells. *Nature.* 2009;460(7259): 1145-1148.
53. Seki T, Yuasa S, Oda M, et al. Generation of induced pluripotent stem cells from human terminally differentiated circulating T cells. *Cell Stem Cell.* 2010;7(1):11-14.

Gene Therapy (2012) 19, 476–482

www.nature.com/gt

ORIGINAL ARTICLE

Interleukin-10 expression induced by adeno-associated virus vector suppresses proteinuria in Zucker obese rats

M Ogura[1,2], M Urabe[1], T Akimoto[2], A Onishi[1,2], C Ito[2], T Ito[3], T Tsukahara[1], H Mizukami[1], A Kume[1], S Muto[2], E Kusano[2] and K Ozawa[1]

Varying degrees of metabolic abnormalities mediated by chronic inflammation are implicated in the chronic glomerular injuries associated with obesity. Interleukin (IL)-10, a pleiotropic cytokine, exerts anti-inflammatory effects in numerous biological settings. In the present study, we explored the biological benefits of adeno-associated virus (AAV) vector-mediated sustained IL-10 expression against the pathological renal characteristics observed in Zucker fatty rats (ZFRs). We injected an AAV vector, encoding rat IL-10 or enhanced green fluorescent protein (GFP) into male ZFRs at 5 weeks of age. Subsequently, the renal pathophysiological changes were analyzed. Persistent IL-10 expression significantly reduced the urinary protein excretion of ZFRs compared with GFP expression (47.1 ± 11.6 mg per mg·creatinine versus 88.8 ± 30.0 mg per mg·creatinine, $P<0.01$). The serum levels of IL-10 negatively correlated with the urinary protein in AAV-treated rats ($r=-0.78$, $P<0.01$). Renal hypertrophy, increased widths in the glomerular basement membrane, and the lack of uniformity and regularity of the foot process of the visceral glomerular epithelial cells of ZFRs were significantly blunted by IL-10 expression. IL-10 also abrogated the downregulation of glomerular nephrin observed in ZFRs treated with the GFP vector. Our findings provide insights into the potential benefit of the anti-inflammatory effects of IL-10 on the overall management of glomerulopathy induced by the metabolic disorders associated with obesity.
Gene Therapy (2012) **19**, 476–482; doi:10.1038/gt.2011.183; published online 24 November 2011

Keywords: obesity; nephrin; glomerular hyperfiltration; glomerular epithelial cells; glucose intolerance

INTRODUCTION

Numerous pathophysiological disorders have been demonstrated to be related to obesity.[1] Not exceptionally, accumulating evidence also suggests a role for obesity in the development of chronic kidney disease.[2–4] The renal effects of obesity in humans and experimental animals include both functional and morphological adaptations, such as an increased glomerular filtration rate, increased renal blood flow, and renal hypertrophy with focal segmental glomerulosclerosis.[5–7] Although the qualitative and quantitative information about the pathogenesis of the glomerulopathy associated with obesity remains to be delineated, varying degrees of metabolic abnormalities appear to be involved. Indeed, hyperinsulinemia resulted in the stimulation of the synthesis of insulin-like growth factors, and the upregulation of transforming growth factor-β1 by elevated serum leptin has been implicated in the chronic glomerulopathy associated with obesity.[8,9] Moreover, hyperlipidemia may also promote glomerulosclerosis through mechanisms in which engagement of lipoprotein receptors on mesangial cells, oxidative cellular injury, macrophage chemotaxis and accelerated synthesis of fibrogenic cytokines are involved.[10]

Interleukin (IL)-10 is a multifunctional cytokine with anti-inflammatory properties.[11] Accumulating evidence suggests potential roles for IL-10 in the management of several pathophysiological disorders, including obesity. Indeed, IL-10 has been shown to not only reduce cholesterol levels, but also to improve the insulin resistance in experimental animal models.[12,13] Moreover, it has also been reported that obese patients and subjects with metabolic syndrome have a lower level of serum IL-10 than healthy normal subjects.[14] These observations led us to consider the therapeutic potential of modulating inflammation by IL-10 in the overall management of obese patients.

In the present study, we evaluated the effects of IL-10 on the renal characteristics of Zucker fatty (Zucker-fa/fa) rats, which have recently been focused on as an experimental animal model of renal injuries mediated by obesity-associated metabolic disorders.[7,15,16] The biological efficiency of the systemic administration of recombinant IL-10 seems to be insufficient because of the immediate decrease resulting from its short bioactive half-life.[17] Instead, we have transferred the gene encoding IL-10 using an adeno-associated virus (AAV) vector, as these vectors can be used to transduce skeletal muscle, thereby inducing the systemic and sustained expression of potentially therapeutic proteins following a single intramuscular administration.[12,18]

RESULTS

The expression of IL-10 in Zucker rats

Our first series of experiments verified the integrity of our vectors in the Zucker-fa/fa rats. The serum concentrations of IL-10 in the rats were determined at 5, 10, 15, 20 and 25 weeks after the initial treatments, which included the administration of phosphate buffer saline (PBS) and transductions of the recombinant AAV type 1-based vector carrying the rat IL-10 (AAV–IL-10) or control-enhanced green fluorescent protein gene (AAV–GFP). As shown in Figure 1,

[1]Division of Genetic Therapeutics, Center for Molecular Medicine, Jichi Medical University, Shimotsuke, Japan; [2]Division of Nephrology, Department of Medicine, Jichi Medical University, Shimotsuke, Japan and [3]Division of Cardiovascular Medicine, Department of Medicine, Jichi Medical University, Shimotsuke, Japan
Correspondence: Dr M Ogura, Division of Nephrology, Department of Internal Medicine, Jichi Medical School, 3311-1 Yakushiji, Shimotsuke-Shi, Tochigi 329-0498, Japan.
E-mail: m-ogura@jichi.ac.jp
Received 25 May 2011; revised 21 September 2011; accepted 17 October 2011; published online 24 November 2011

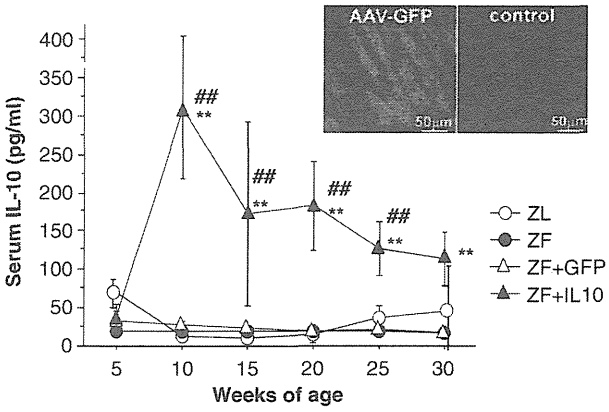

Figure 1 The longitudinal changes in serum concentrations of IL-10 at 5, 10, 15, 20 and 25 weeks after the initial sham treatments (PBS alone), and transductions of AAV–IL-10 or AAV–GFP into the Zucker fa/fa rats or lean littermates. Inset: an analysis of the cryostat sections of the anterior tibial muscles injected with AAV–GFP or PBS (control). The immunofluorescence analyses performed 10 weeks post-vector injections revealed ubiquitous GFP expression within the muscle tissue, thus suggesting efficient gene transduction by the AAV vectors. Scale bar is indicated in each panel. The data are the means ± s.d. (n=6). $^{**}P<0.01$ versus ZF and ZF+GFP groups; $^{\#\#}P<0.01$ versus the value at 5 weeks of age.

statistically significant increases in serum IL-10 were confirmed in Zucker-fa/fa rats administered AAV–IL-10 (sham Zucker-fa/fa rats administered PBS (ZF)+IL-10), whereas the levels in Zucker-fa/fa rats administered AAV–GFP (ZF+GFP), ZF and control Zucker lean littermates (Zucker +/+) administered PBS (ZL) were comparable. The levels of IL-10 in ZF+IL-10 were about 12-fold higher at week 5, and an average of 5-fold higher than ZF, ZF+GFP and ZL groups at 25 weeks after the initial treatments.

The effects of IL-10 on clinical and laboratory characteristics

The body weights of all rats were increased during the observation period. Although the degree of the increases was significantly higher in the Zucker-fa/fa rats than in the ZL rats, the mean body weights of ZF, ZF+GFP and ZF+IL-10 at each time point were comparable (Figure 2a). Similarly, the food consumption of the Zucker-fa/fa rats was significantly greater than that of the ZL, although there were no significant differences in the amount of food intake in the three Zucker-fa/fa rat groups (Figure 2b). On the other hand, the serum levels of total cholesterol (Tcho) and triglycerides (TG) were significantly higher in Zucker-fa/fa rats compared with ZL throughout the observation period. However, in the ZF+IL-10, the serum Tcho was significantly lower than those in the ZF and ZF+GFP (Figure 2c). Similar trends were also confirmed in the longitudinal changes in the serum TG. As shown in Figure 2d, Zucker-fa/fa rats had significantly higher serum TG than their lean littermates; however, the expression of IL-10 seemed to negatively affect the level of TG. At 30 weeks of age, these parameters negatively correlated with the IL-10 level in the Zucker-fa/fa rats with PBS or AAV treatment (Figures 2e and f). During the observation period, no significant difference in the systolic blood pressure was observed in the Zucker-fa/fa rats treated with PBS or the AAV, although there was a trend for the systolic blood pressure in the ZL to be higher than that of all of the Zucker-fa/fa rats (data not shown).

We next analyzed the effect of IL-10 on the parameters related to the glucose metabolism. As shown in Table 1, the fasting blood glucose levels of Zucker-fa/fa rats were significantly higher at 10 weeks after the administration of the vector with GFP or PBS administration compared with the lean littermates. At 30 weeks of age, we determined the blood hemoglobin A1c (HbA1c) and serum immuno-reactive insulin levels. As shown in Figure 3a, the transduction of IL-10 reversed the increase in the levels of HbA1c that was confirmed in ZF and ZF+GFP rats, thus suggesting that IL-10 might have a role in improving the disturbance of the fed-state glucose metabolism in the Zucker fa/fa rats. Indeed, the fed state serum insulin level was significantly elevated in ZF+IL-10 rats compared with the other groups, whereas the levels of fasting serum insulin in the Zucker-fa/fa rats were comparable (Figure 3b).

The effects of IL-10 on renal characteristics

We also explored the effects of IL-10 on the renal characteristics of the obese rats. As shown in Figure 4a, all three groups of obese rats (ZF, ZF+GFP and ZF+IL-10) demonstrated a gradual increase in urinary protein in a time-dependent manner, and the urinary protein level in the ZF and ZF+GFP finally increased up to 102.2 ± 21.9 and 88.8 ± 30.0 mg per mg·creatinine, respectively. At 30 weeks of age, the urinary protein in the ZF+IL-10 (47.1 ± 11.6 mg per mg·creatinine) was significantly lower than in the other Zucker-fa/fa rats groups ($P<0.01$). Moreover, the serum levels of IL-10 negatively correlated with the urinary protein level in Zucker-fa/fa rats ($r=-0.88$, $P<0.01$, $n=17$; Figure 4b). During the observation period, the creatinine clearance (Ccr) in obese rats without IL-10 was significantly increased at both 25 and 30 weeks of age (Figure 4c). There was also a negative correlation between the serum IL-10 level and Ccr ($r=-0.65$, $P<0.01$, $n=15$; Figure 4d).

Figure 5 shows the anatomical and morphological effects of IL-10 on the Zucker-fa/fa rats. All three groups of Zucker-fa/fa rats had significantly higher kidney weights than the ZL at 30 weeks of age. However, the expression of IL-10 caused a significant decrease in the kidney weight when compared with the ZF and ZF+GFP (1.70 ± 0.13 g versus 1.86 ± 0.12 g, $P<0.05$, and 1.85 ± 0.09 g, $P<0.05$, respectively; Figure 5a). When viewed under a light microscope, there were no apparent histological changes compatible with glomerulosclerosis and cellular infiltrations within the glomerulus in any of the subjects; however, the Zucker-fa/fa rats had a larger area of glomeruli than the ZL, which was significantly reduced by the persistent expression of IL-10 in the ZF+IL-10 (Figures 5b and c). Transmission electron microscopy showed the hyperplastic glomerular basement membrane (GBM) and prominent foot process effacement in ZF and ZF+GFP (Figure 5b), but these changes seemed to be prevented or reversed in the ZF+IL-10. Indeed, there were significant differences in the mean width of the GBM between the ZF+IL-10 and the other two groups of Zucker-fa/fa rats (Figure 5d). The lack of uniformity and regularity of the foot process demonstrated by scanning electron microscopic was remarkable in the ZF and ZF+GFP, but this was not observed in the ZF+IL-10 and ZL (Figure 5b).

The effects of IL-10 on the expression of nephrin within the glomeruli of Zucker-fa/fa rats

To determine the potential mechanisms of the counter-effect of IL-10 on the changes in the renal characteristics in the Zucker-fa/fa rats, we evaluated the effects of IL-10 on the expression of nephrin within glomeruli. As shown in Figure 6, the glomerular nephrin expressions in Zucker fa/fa rats treated with PBS or AAV–GFP were significantly diminished compared with that of lean littermates, and the transduction of IL-10 apparently reversed the reduced expression of nephrin within glomeruli that was observed in the Zucker-fa/fa rats (Figure 6).

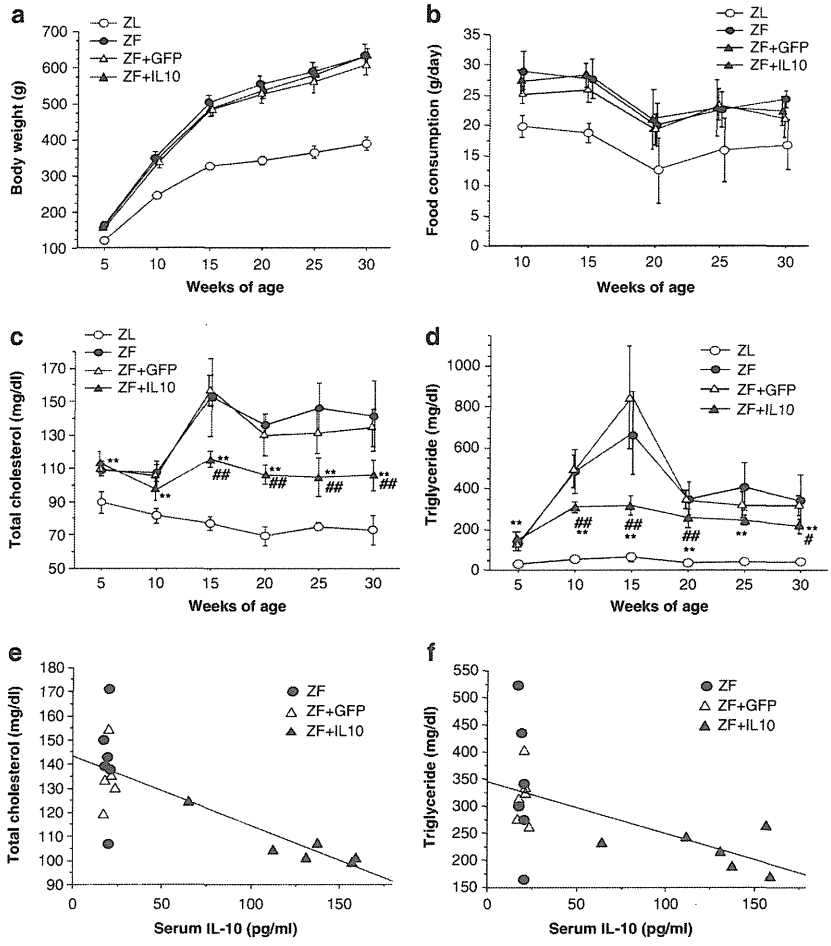

Figure 2 The changes in the body weights (**a**), food consumption (**b**), serum Tcho (**c**) and serum TG (**d**). The body weights and food consumption were significantly higher in obese rats than in lean littermates at each point time. Note that the body weights and the food consumption in the three groups of obese rats were comparable, whereas the serum Tcho and TG levels were significantly lower than those in the ZF and ZF+GFP groups. The data are the means ± s.d. (n=6). $^{**}P<0.01$ versus the control; $^{\#}P<0.05$, $^{\#\#}P<0.01$ versus ZF and ZF+GFP groups. The relationships between IL-10 and Tcho (**e**) and TG (**f**) were also evaluated (groups: ZF, ZF+GFP and ZF+IL-10; n=6 per group; r=−0.77, $P<0.01$ and r=−0.77, $P<0.01$, respectively).

Table 1 Changes in FBS in Zucker fa/fa rats and age-matched control lean littermates

Age (weeks)	*ZL*	*ZF*	*ZF+GFP*	*ZF+IL-10*
10	127.2 ± 12.1	157.5 ± 21.0[a]	175.5 ± 19.6[a]	175.8 ± 24.5[a]
20	120.2 ± 7.3	126.3 ± 13.5	129.2 ± 11.5	139.2 ± 22.1[a]
30	108.8 ± 14.3	118.7 ± 16.3	135.3 ± 20.0[a]	126.8 ± 10.8[a]

Abbreviations: FBS, fasting blood glucose; GFP, green fluorescent protein; IL, interleukin; ZF, sham Zucker-fa/fa rats administered PBS; ZL, Zucker lean littermates (Zucker +/+) administered PBS. [a]$P<0.05$ versus ZL.

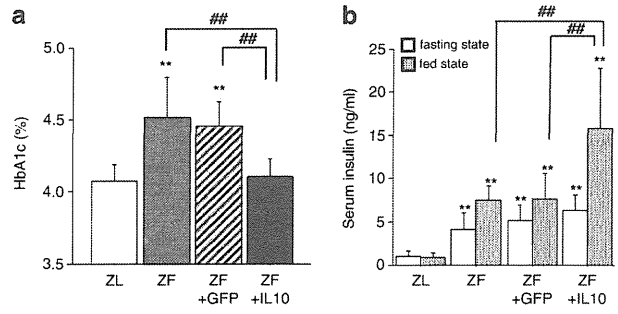

Figure 3 The effect of the IL-10 expression on the level of blood HbA1c (**a**) and serum immunoreactive insulin (**b**). The data were determined with blood samples obtained from rats at 30 weeks of age. $^{**}P<0.01$ versus the control and $^{\#\#}P<0.01$, respectively.

DISCUSSION

The present study clearly demonstrates for the first time that IL-10, delivered by an AAV vector, suppresses the changes in renal characteristics in obese rats, including the increase in urinary protein, elevated Ccr, glomerular hypertrophy and the decreased glomerular expression of nephrin, without affecting the body weight and food intake of the rats. These results suggest the potential benefits of IL-10 in the management of obese subjects with renal pathophysiological abnormalities.

Numerous studies have focused on the abnormalities in lipid metabolism as a potential mechanism underlying various types of glomerular injuries, and the treatment of hyperlipidemia has been shown to reduce the excretion of urinary proteins and to decrease the

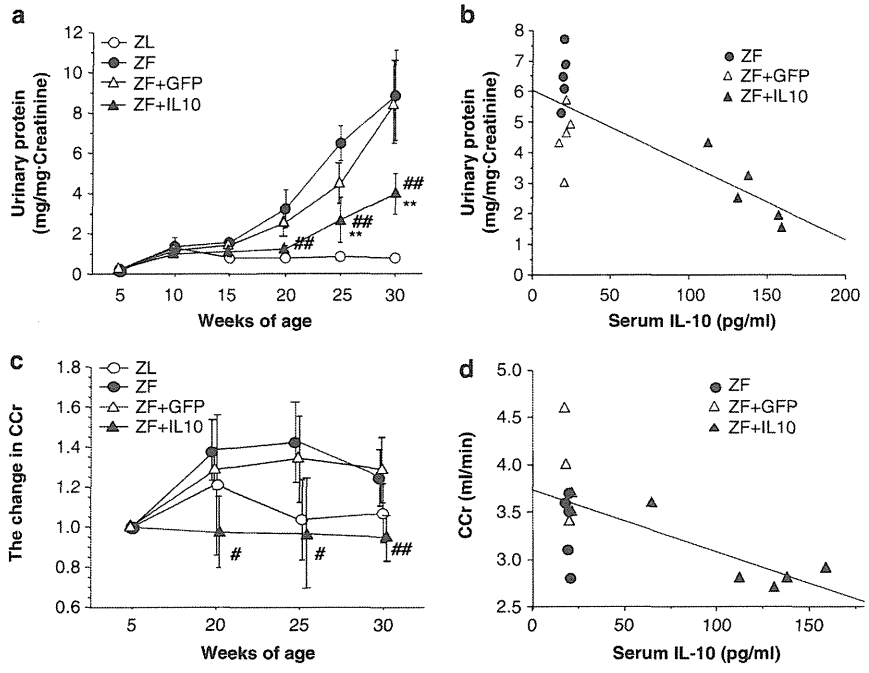

Figure 4 The effects of the IL-10 expression on urinary protein excretion (**a**) and the changes in the Ccr (**c**) in the ZF (●), ZF+GFP (▲), ZF+IL-10 (▲) and ZL (○) rats. The data are the means ± s.d. (n=5–6). $^{**}P<0.01$ versus the controls; $^{\#}P<0.05$, $^{\#\#}P<0.01$ versus ZF or ZF+GFP groups. The relationship between IL-10 and the urinary protein excretion (**b**) or the change in the Ccr (**d**) in the obese rats (groups: ZF, ZF+GFP or ZF+IL-10; n=5–6 per group; r=−0.78, $P<0.01$ and r=−0.65, $P<0.01$, respectively).

glomerular injury characterized by mesangial matrix expansion and focal segmental glomerulosclerosis, which are typical of Zucker fa/fa rats at about 60 weeks of age, without any changes in glomerular hemodynamic function.[7,10,16,19] As such renal structural alterations seem to be relatively nonspecific and may represent part of a common final pathway,[15] we focused on the changes in renal characteristics that precede the development of mesangial matrix expansion and focal segmental glomerulosclerosis. Consistently, the histological analyses of our Zucker fa/fa rats performed at 30 weeks of age failed to demonstrate such glomerular lesions. Instead, glomerular hypertrophy, an increase in the widths of the GBM and the elevation of Ccr due to presumable glomerular hyperfiltration, which have all been implicated in hyperglycemia and are considered to be early events followed by diabetic glomerulosclerosis among diabetic subjects,[20–22] were observed.

These findings might not be surprising, as abnormal glucose metabolism characterized by mild hyperglycemia, as well as hyperinsulinemia and insulin resistance, are alternative metabolic characteristics of Zucker fa/fa rats.[7,15,23] Obviously, this was also the case with the present study. Of note, IL-10 seems to improve the disturbed fed-state glucose metabolism of the Zucker fa/fa rats, as the HbA1c in ZF-IL-10 rats was significantly decreased compared with the rest of the obese groups. The recovery from advanced insulin resistance is unlikely to be implicated in these rats. Instead, the accelerated increase in serum insulin seems to be involved in the countervailing effect of IL-10 on the glucose intolerance. Such an increase in serum insulin may be attributable to a change in the metabolic clearance or altered sensitivity to blood glucose. Alternatively, IL-10 might stimulate pancreatic β-cell function.[24] Although the elevation of serum insulin seemed to be necessary for glycemic control among our obese animals, one may argue that this might have adverse consequences on the renal tissue, and thus, might contribute to the development of a wide range of glomerular and interstitial injuries associated with disturbed glucose metabolism.

Indeed, it has been shown that hyperinsulinemia pleiotropically affects the kidney tissue through various pathways.[8,9,25] Nevertheless, renal pathophysiological evaluations failed to confirm the adverse effect of hyperinsulinemia in ZF-IL10 rats. Our results suggest that the biological significance of the improvement in glucose intolerance, mediated by the further increase in serum insulin induced by IL-10, on the renal characteristics of Zucker fa/fa rats should exceed that of hyperinsulinemia. Otherwise, an alternative process independent of the regulation of obesity-related metabolic disturbance might be involved in the countervailing effect of IL-10 on the renal pathophysiological characteristics among our obese animals.

Whether the glomerular morphological changes demonstrated in the present study cause or contribute to the presumable development of mesangial matrix expansion and focal segmental glomerulosclerosis in Zucker-fa/fa rats, which have been demonstrated to have abnormal lipid metabolism at ages older than 30 weeks,[7,10,16,19] remains to be determined. However, the fact that there were significant decreases in the serum levels of Tcho and TG in the ZF+IL-10 rats led us to consider that the early phase of the changes in the renal characteristics of Zucker fa/fa rats might be modulated, at least in part, by IL-10 through the reduction of Tcho and TG. Although the course of the etiological linkage between IL-10 and TG remains to be delineated, previous data suggest that IL-10 might have a direct effect on the cholesterol metabolism through the suppression of the hydroxymethylglutaryl-CoA reductase expression, thereby lowering the Tcho level.[12]

A hyperplastic GBM is often accompanied by changes in the visceral glomerular epithelial cells, that is, podocytes, and a progressive loss of podocyte foot processes associates with narrowing of the filtration slits, whereas the number of podocytes decreases with the increase in

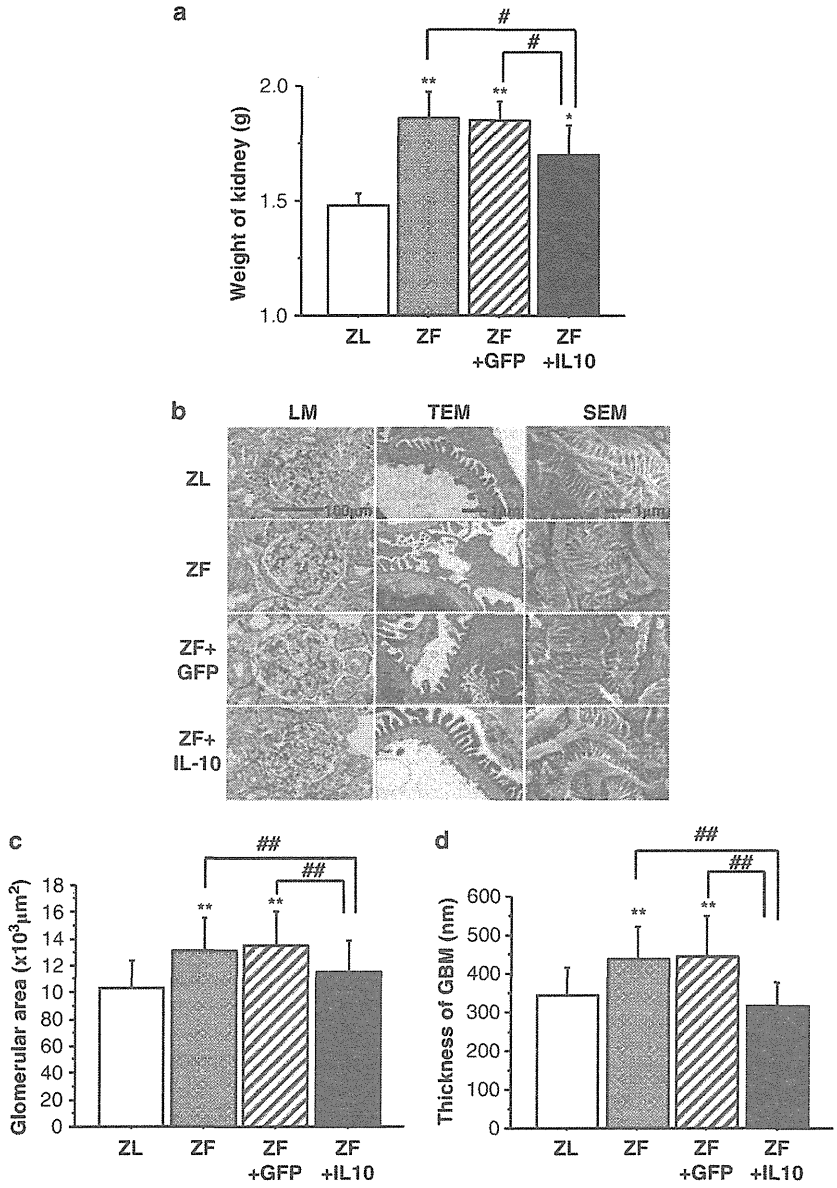

Figure 5 The effects of IL-10 expression on the renal morphological changes in ZFRs. (**a**) The changes in the weights of the kidneys of ZF (black hatched box), ZF+GFP (black striped box), ZF+IL-10 (black box) and ZL (white box) rats. The results were presented as means ± s.d. (n=5). $^{*}P<0.05$, $^{**}P<0.01$, versus the controls; $^{\#}P<0.05$ versus the ZF and ZF+GFP groups. (**b**) Representative photomicrographs of periodic acid-Schiff-stained light microscopic, transmission electron microscopy and scanning electron microscopic views. The scale bars are shown in the panel for the control lean littermates. (**c**) The differences in the glomerular area of the ZF (black hatched box), ZFtGFP (black striped box), ZFtIL-10 (black box) and ZL (white box) rats. (**d**) The differences in the width of the GBM of ZF (black hatched box), ZFtGFP (black striped box), ZFtIL-10 (black box) and ZL (white box) rats. The results are presented as the means ± s.d. $^{**}P<0.01$ versus the controls; $^{\#\#}P<0.01$ versus the ZF and ZF ± GFP groups.

urinary protein excretion.[26,27] Although the precise number of podocytes was not quantified in the present study, such pathogenic processes were likely modulated by IL-10, as the prominent foot process effacement associated with the hyperplastic GBM, and the lack of uniformity and regularity of the foot process confirmed in ZF and ZF-GFP were recovered in ZF+IL-10. Moreover, IL-10 remarkably blunted the reduced glomerular expression of nephrin, which has been located to the slit diaphragm of glomerular podocytes, where it acts as a renal ultrafilter barrier function.[28] Although the mechanism leading to the downregulation of glomerular nephrin in our rats is not well characterized, the potential role of reactive oxygen species, and particularly, the balance of lipid peroxidase, was recently proposed to account for the decrease in nephrin mRNA in experimental glomerulopathy.[29] Therefore, it is reasonable to consider that IL-10 should directly or indirectly modulate such pathophysiological processes within our obese subjects.

Although the present study provides information regarding the effects of IL-10 on the renal characteristics of the Zucker fa/fa rats, our results should be interpreted within the context of the study's limitations. First, the number of animals included in each group was small, implying that the study may be underpowered for the evaluation of several parameters, and selection bias may also be present. Indeed, our

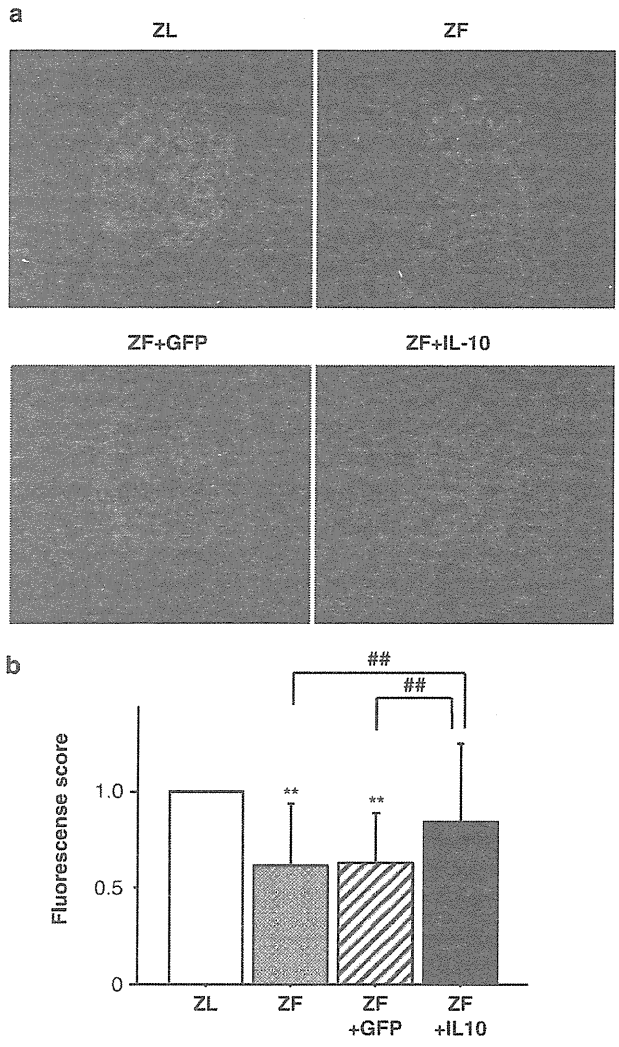

Figure 6 Immunofluorescent staining of glomerular nephrin from ZFRs and control littermates. (**a**) Representative microscopic views are shown. (**b**) The fluorescence intensity of each view was also quantified using arbitrary units. $^{**}P<0.01$ versus control littermates; $n=6$; $^{\#\#}P<0.01$ versus the ZF and ZF+GFP groups.

findings, demonstrating that the mean body weights and the food consumption levels of each of the obese groups, might have been underestimated, as it has been reported that IL-10 could attenuate the changes in food intake and energy expenditure in the experimental rat model of acute inflammatory disturbance associated with bacterial infection.[30] It may be interesting to determine whether the IL-10 treatment applied to our obese rats affected their glucose and lipid metabolism without inducing any change in their body weight and food consumption. Whether our findings remain true when the number of subjects is increased should be evaluated in greater detail in a future study.

In summary, AAV vector-mediated IL-10 gene transfer into the Zucker fa/fa rats could introduce efficient and stable IL-10 expression, resulting in the marked reduction of urinary protein excretion. These changes were associated with the recovery of renal structural alterations. Our observations indicate the presence of complex interactions between the changes in the renal characteristics of Zucker fa/fa rats and the inflammatory cascade, as well as the potential benefit of the anti-inflammatory effects of IL-10 in the overall management of glomerulopathy mediated by obesity-related metabolic disorders.

METHODS

AAV vector production

DNA encoding rat IL-10 was PCR-amplified from rat splenocyte complementary DNA as described previously, using the primers 5′-GCACGAGAGCCAC AACGCa-3′ and 5′-GATTTGAGTACGATCCATTTATTCAAAACGAGGAT-3′.[18] For efficient transgene expression in the skeletal muscle, we constructed a recombinant AAV type 1 vector, which carried the *IL-10* gene or *GFP* gene, controlled by the modified chicken β-actin promoter with the cytomegalovirus posttranscriptional regulatory element (a generous gift from Dr Thomas Hope, Infectious Disease Laboratory, Salk Institute). AAV vectors were prepared according to the previously described three-plasmid transfection adenovirus-free protocol, with minor modification to use the active gassing system.[18,31] Briefly, 60% confluent human embryonic kidney 293 cells incubated in a large culture vessels were co-transfected with the proviral transgene plasmid, AAV-1 chimeric helper plasmid (p1RepCap), and the adenoviral helper plasmid pAdeno (Avigen Inc., Alameda, CA, USA).[31] The crude viral lysates were purified by two rounds of CsCl in a two-tier centrifugation. The titer of the viral stock was determined against plasmid standards by using dot blot hybridization, after which the stock was diluted in PBS before injection.

Animal model and experimental design

All animal procedures were approved by the Jichi Medical University ethics committee and were performed in accordance with the National Institutes of Health Guide for the Care and Use of Laboratory Animals. Male Zucker-fa/fa and Zucker +/+ rats were obtained from Japan SLC Inc (Shizuoka, Japan). Animals were housed in a temperature and humidity controlled room, and standard rat chow (CE-2, Clea Japan, Inc., Tokyo, Japan) and water were available *ad libitum*. Five-week-old male Zucker-fa/fa rats were randomly divided into three groups ($n=6$ in each group): that is, ZF, ZF+GFP and ZF+IL-10. Control lean littermates administered PBS (ZL) were also included in the study. Under ether anesthesia, the PBS buffer or AAV vectors in PBS were injected into the bilateral anterior tibial muscles of the rats (200 μl per site, 1×10^{11} genome copies per rat). For each animal, body weight and food consumption were measured at 5, 10, 15, 20, 25 and 30 weeks of age. Urinary samples were collected in metabolic sampling bottles over 24 h. Blood samples were collected by tail clipping under ether anesthesia after the rats had fasted for 16 h. In some circumstances, morning blood samples were also collected to determine the fed-state blood glucose and serum immunoreactive insulin levels. The serum levels of Tcho (Cholesterol C-test; Wako Chemicals, Tokyo, Japan), TG (L-Type TG H Kit; Wako Chemicals) and IL-10 (Quantikine ELISA Kit; R&D systems, Minneapolis, MN, USA) were determined according to the manufacturer's instructions. The levels of glucose (Shino-Test, Tokyo, Japan) and HbA1c (RAPIDIA Auto HbA1c-L; Fujirebio, Inc., Tokyo, Japan) were determined with whole blood samples. The immunoreactive serum insulin level was determined using a commercial radioimmunoassay kit (Rat insulin RIA kit; Linco Research, Inc., St Charles, MO, USA) with rat insulin as the standard. Systolic blood pressure was measured by the non-invasive tail-cuff method using a manometer–tachometer system (MK-2000, Muromachi Kikai, Tokyo, Japan). The amount of urinary protein excretion for 24 h was determined with TP-HR II Wako reagent (Wako Chemicals). Serum creatinine and urinary creatinine were measured with the creatinine reagent (Alfresa Pharma Corporation, Osaka, Japan), using an automated analyzer (Hitachi-7180, Hitachi High-Technologies, Tokyo, Japan). We calculated the Ccr using the following equation: Ccr (ml min^{-1})=urinary creatinine (mg dl^{-1}) × urine flow rate (ml min^{-1})/serum creatinine (mg dl^{-1}).

Light microscopy

At 30 weeks of age, the anesthetized rats were perfused with 100 ml of saline. For evaluation of light microscopic findings, the kidneys were fixed in 10% paraformaldehyde in PBS (pH 7.4) and finally embedded in paraffin, sectioned, and analyzed for histology. Then, 3-μm sections were subjected to periodic acid-Schiff staining. The mean glomerular tuft volume was determined by the

images from 50 consecutive glomerular cross sections, which were collected for each of the histological sections using an Olympus BX50 light microscope (Olympus, Tokyo, Japan). The area of each glomerular profile was measured manually by tracing the glomerular outline on a computer screen, and the size of each area was calculated by computerized morphometry (Image-Pro plus, Media Cybernetics, Inc., Bethesda, MD, USA). The measurements were performed in a blinded fashion.

Electron microscopy

For transmission electron microscopy, tissues of the left kidneys fixed with 2.5% glutaraldehyde in phosphate buffer (pH 7.4) were postfixed in 2% osmium tetroxide for 2 h at 4 °C. Then, samples were dehydrated in a graded series of ethanol solutions at room temperature, and embedded in Quetol 812 (Nisshin EM Co., Tokyo, Japan). Thin sections of 80 nm were contrasted with 4% uranyl acetate for 15 min and subsequently stained with lead citrate for 5 min at room temperature. Samples were finally examined using a transmission electron microscope (H-7500, Hitachi High-Technologies). The mean width of the GBM was determined by the images of 100 consecutive glomerular sections obtained from two subjects in each group. For scanning electron microscopic examination, small pieces of the kidney cortex were fixed in 2.5% glutaraldehyde in sodium cacodylate buffer (pH 7.4) for 2 h, and subsequently postfixed in 1% osmium tetroxide. Specimens were then dehydrated in a series of ethanols of increasing concentrations, and critical point dried. Once mounted onto specimen holders and desiccated, the samples were sputter-coated with a layer of gold and examined with a S-4300 scanning electron microscope (Hitachi High-Technologies), and images were collected at standard settings.

Immunofluorescent staining

The analysis of nephrin expression in the renal cortex was performed using an immunofluorescence technique. The snap-frozen sections of 3 μm, fixed in 1% formaldehyde and blocked in 5% normal goat serum, were incubated with rabbit anti-nephrin primary antibodies (Immuno-biological Laboratories Co., Ltd., Gunma, Japan) and washed twice with PBS. Subsequently, sections were also incubated with Alexa Fluor 488-conjugated anti-rabbit antibodies (Invitrogen, Carlsbad, CA, USA). Stained sections were examined using a PROVIS AX-80 optical microscope (Olympus). The results were calculated as the intensity of fluorescence within the glomerular tuft by using the Image J 1.42q software package (National Institutes of Mental Health, Bethesda, MD, USA). On average, over 30 randomly selected hilar glomerular tuft cross-sections were assessed per rat.

Statistical analysis

The results were expressed as the means ± s.d. of the mean. The data were analyzed by an analysis of variance combined with Fisher's protected least significant difference. Differences with $P<0.05$ were considered to be statistically significant. The correlation test was used to measure the association between two variables, if appropriate.

CONFLICT OF INTEREST

The authors declare no conflict of interest.

ACKNOWLEDGEMENTS

Part of the work presented in the original manuscript was presented in abstract in the Renal Week 2009 (Annual Meeting of the American Society of Nephrology). We sincerely thank Takashi Yashiro for conducting the electron microscopy studies, and Tom Kouki for his technical assistance in tissue processing for histological and ultrastructural studies.

1 Kambham N, Markowitz GS, Valeri M, Lin J, D'Agati VD. Obesity-related glomerulopathy: an emerging epidemic. *Kidney Int* 2001; **39**: 1498–1509.
2 Ramirez SP, McClellan W, Port FK, Hsu SIH. Risk factors for proteinuria in a large, multiracial, Southeast Asian population. *J Am Soc Nephrol* 2002; **1**: 1907–1917.
3 Iseki K, Ikemiya K, Kinjo K, Inoue T, Iseki C, Takishita S. Body mass index and the risk of development of end-stage renal disease in a screened cohort. *Kidney Int* 2004; **65**: 1870–1876.
4 Hallan S, de Mutsert R, Carlsen S, Dekker FW, Aasarod K, Holmen J. Obesity, smoking, and physical inactivity as risk factors for CKD: are men more vulnerable? *Am J Kidney Dis* 2006; **47**: 396–405.
5 Chagnac A, Weinstein T, Herman M, Hirsh J, Gafter U, Ori Y. The effects of weight loss on renal function in patients with severe obesity. *J Am Soc Nephrol* 2003; **14**: 1480–1486.
6 Chen HM, Li SJ, Chen HP, Wang QW, Li LS, Liu ZH. Obesity-related glomerulopathy in China: a case series of 90 patients. *Am J Kidney Dis* 2008; **52**: 58–65.
7 Kasiske BL, Cleary MP, O'Donnell MP, Keane WF. Effects of genetic obesity on renal structure and function in the Zucker rat. *J Lab Clin Med* 1985; **106**: 598–604.
8 Frystyk J, Skjaerbaek C, Vestbo E, Fisker S, Orskov H. Circulating levels of free insulin-like growth factors in obese subjects: the impact of type 2 diabetes. *Diabetes Metab Res Rev* 1999; **15**: 314–322.
9 Wolf G, Hamann A, Han DC, Helmchen U, Thaiss F, Ziyadeh FN *et al.* Leptin stimulates proliferation and TGF-beta expression in renal glomerular endothelial cells. potential role in glomerulosclerosis. *Kidney Int* 1999; **56**: 860–872.
10 Keane WF. Lipids and the kidney. *Kidney Int* 1994; **46**: 910–920.
11 Mu W, Ouyang X, Agarwal A, Zhang L, Long DA, Cruz PE *et al.* IL-10 suppresses chemokines, inflammation, and fibrosis in a model of chronic renal disease. *J Am Soc Nephrol* 2005; **16**: 3651–3660.
12 Yoshioka T, Okada T, Maeda Y, Ikeda U, Shimpo M, Nomoto T *et al.* Adeno-associated virus vector-mediated interleukin-10 gene transfer inhibits atherosclerosis in apolipoprotein E-deficient mice. *Gene Therapy* 2004; **11**: 1772–1779.
13 Hong EG, Ko HJ, Cho YR, Kim HJ, Ma Z, Yu TY *et al.* Interleukin-10 prevents diet-induced insulin resistance by attenuating macrophage and cytokine response in skeletal muscle. *Diabetes* 2009; **58**: 2525–2535.
14 Esposito K, Pontillo A, Giugliano F, Giugliano G, Marfella R, Nicoletti G *et al.* Association of low interleukin-10 levels with the metabolic syndrome in obese women. *J Clin Endocrinol Metab* 2003; **88**: 1055–1058.
15 Coimbra TM, Janssen U, Grone HJ, Ostendorf T, Kunter U, Schmidt H *et al.* Early events leading to renal injury in obese Zucker (fatty) rats with type II diabetes. *Kidney Int* 2000; **57**: 167–182.
16 Kasiske BL, O'Donnel MP, Cleary MP, Keane WF. Treatment of hyperlipidemia reduces glomerular injury in obese Zucker rats. *Kidney Int* 1988; **33**: 667–672.
17 Li MC, He SH. IL-10 and its related cytokines for treatment of inflammatory bowel disease. *World J Gastroenterol* 2004; **10**: 620–625.
18 Ito T, Okada T, Miyashita H, Nomoto T, Nonaka-Sarukawa M, Uchibori R *et al.* Interleukin-10 expression mediated by an adeno-associated virus vector prevents monocrotaline-induced pulmonary arterial hypertension in rats. *Circ Res* 2007; **101**: 734–741.
19 Alderson NL, Chachich ME, Youssef NN, Beattie RJ, Nachtigal M, Thorpe SR *et al.* The AGE inhibitor pyridoxamine inhibits lipemia and development of renal and vascular disease in Zucker obese rats. *Kidney Int* 2003; **63**: 2123–2133.
20 Tsilibary EC. Microvascular basement membranes in diabetes mellitus. *J Pathol* 2003; **200**: 537–546.
21 Caramori ML, Kim Y, Huang C, Fish AJ, Rich SS, Miller ME *et al.* Cellular basis of diabetic nephropathy: 1. Study design and renal structural-functional relationships in patients with long-standing type 1 diabetes. *Diabetes* 2002; **51**: 506–513.
22 Akimoto T, Ito C, Saito O, Takahashi H, Takeda S, Ando Y *et al.* Microscopic hematuria and diabetic glomerulosclerosis—clinicopathological analysis of type 2 diabetic patients associated with overt proteinuria. *Nephron Clin Pract* 2008; **109**: c119–c126.
23 Fürnsinn C, Komjati M, Madsen OD, Schneider B, Waldhäusl W. Lifelong sequential changes in glucose tolerance and insulin secretion in genetically obese Zucker rats (fa/fa) fed a diabetogenic diet. *Endocrinology* 1991; **128**: 1093–1099.
24 Sandler S, Welsh N. Interleukin-10 stimulates rat pancreatic islets *in vitro*, but fails to protect against interleukin-1. *Biochem Biophys Res Commun* 1993; **195**: 859–865.
25 Sarafidis PA, Ruilope LM. Insulin resistance, hyperinsulinemia, and renal injury: mechanisms and implications. *Am J Nephrol* 2006; **26**: 232–244.
26 Bjorn SF, Bangstad HJ, Hanssen KF, Nyberg G, Walker JD, Viberti GC *et al.* Glomerular epithelial foot processes and filtration slits in IDDM patients. *Diabetologia* 1995; **38**: 1197–1204.
27 Herbach N, Schairer I, Blutke A, Kautz S, Siebert A, Goke B *et al.* Diabetic kidney lesions of $GIPR^{dn}$ transgenic mice: podocyte hypertrophy and the thickening of the GBM precede glomerular hypertrophy and glomerulosclerosis. *Am J Physiol Renal Physiol 2009*; **296**: F819–F829.
28 Bonnet F, Cooper ME, Kawachi H, Allen TJ, Boner G, Cao Z. Irbesartan normalizes the deficiency in glomerular nephrin expression in a model of diabetes and hypertension. *Diabetologia* 2001; **44**: 874–877.
29 Luimula P, Ahola H, Wang SX, Solin ML, Aaltonen P, Tikkanen I *et al.* Nephrin in experimental glomerular disease. *Kidney Int* 2000; **58**: 1461–1468.
30 Hollis JH, Lemus M, Evetts MJ, Oldfield BJ. Central interleukin-10 attenuates lipopolysaccharide-induced changes in food intake, energy expenditure and hypothalamic Fos expression. *Neuropharmacology* 2010; **58**: 730–738.
31 Okada T, Nomoto T, Yoshioka T, Nonaka-Sarukawa M, Ito T, Ogura T *et al.* Large-scale production of recombinant viruses by use of a large culture vessel with active gassing. *Hum Gene Ther* 2005; **16**: 1212–1218.

J Clin Immunol (2012) 32:39–49
DOI 10.1007/s10875-011-9600-0

Successful Treatment with Infliximab for Inflammatory Colitis in a Patient with X-linked Anhidrotic Ectodermal Dysplasia with Immunodeficiency

Tomoyuki Mizukami · Megumi Obara · Ryuta Nishikomori · Tomoki Kawai · Yoshihiro Tahara · Naoki Sameshima · Kousuke Marutsuka · Hiroshi Nakase · Nobuhiro Kimura · Toshio Heike · Hiroyuki Nunoi

Received: 23 July 2011 / Accepted: 15 September 2011 / Published online: 13 October 2011

Abstract X-linked anhidrotic ectodermal dysplasia with immunodeficiency (X-EDA-ID) is caused by hypomorphic mutations in the gene encoding nuclear factor-κB essential modulator protein (NEMO). Patients are susceptibile to diverse pathogens due to insufficient cytokine and frequently show severe chronic colitis. An 11-year-old boy with X-EDA-ID was hospitalized with autoimmune symptoms and severe chronic colitis which had been refractory to immunosuppressive drugs. Since tumor necrosis factor (TNF) α is responsible for the pathogenesis of NEMO colitis according to intestinal NEMO and additional TNFR1 knockout mice studies, and high levels of TNFα-producing mononuclear cells were detected in the patient due to the unexpected gene reversion mosaicism of NEMO, an anti-TNFα monoclonal antibody was administered to ameliorate his abdominal symptoms. Repeated administrations improved his colonoscopic findings as well as his dry skin along with a reduction of TNFα-expressing T cells. These findings suggest TNF blockade therapy is of value for refractory NEMO colitis with gene reversion.

Keywords NEMO colitis · infliximab · gene reversion

Introduction

X-linked anhidrotic ectodermal dysplasia with immunodeficiency (X-EDA-ID) is a rare inherited disease caused by hypomorphic mutations in the gene encoding nuclear factor-κB

Electronic supplementary material The online version of this article (doi:10.1007/s10875-011-9600-0) contains supplementary material, which is available to authorized users.

T. Mizukami · M. Obara · H. Nunoi (✉)
Division of Pediatrics, Department of Reproductive and Developmental Medicine, Faculty of Medicine, University of Miyazaki,
5200 Kihara, Kiyotake,
Miyazaki 889-1692, Japan
e-mail: h-nunoi@fc.miyazaki-u.ac.jp

T. Mizukami
Kumamoto Saishunso National Hospital,
Kumamoto, Japan

R. Nishikomori · T. Kawai · T. Heike
Department of Pediatrics,
Kyoto University Graduate School of Medicine,
Kyoto, Japan

Y. Tahara
Department of Gastroenterology and Hematology, Faculty of Medicine, University of Miyazaki,
Miyazaki, Japan

N. Sameshima · K. Marutsuka
Department of Pathophysiology, Faculty of Medicine, University of Miyazaki,
Miyazaki, Japan

H. Nakase
Department of Gastroenterology and Hepatology,
Kyoto University Graduate School of Medicine,
Kyoto, Japan

N. Kimura
Division of Medical Oncology, Hematology and Infectious Disease, Department of Medicine, Fukuoka University,
Fukuoka, Japan

(NF-κB) essential modulator (NEMO), which is the regulatory subunit of IκB kinase [1–3]. Mutations of NEMO can cause an impaired capacity to activate NF-κB, resulting in defects in ectodermal differentiation and innate and adaptive immunity [4, 5]. Affected patients generally show multiple developmental anomalies in ectodermal tissues such as sparse hair, hypodontia with conical teeth, and anhidrosis or hypohidrosis due to lack of sweat glands. These patients also suffer from severe life-threatening infections in various sites caused by Gram-positive or Gram-negative bacteria or mycobacteria. Immunological abnormalities are characterized by defects in the production of proinflammatory cytokines in response to lipopolysaccharide (LPS) stimulation, hypogammaglobulinemia, specific antibody deficiency, and natural killer cell dysfunction. Hematopoietic stem cell transplantation for X-EDA-ID has been employed as a curative treatment [6–10], but has sometimes resulted in engraftment failure.

NEMO colitis, which is inflammatory colitis associated with mutated NEMO protein [11], is found in one fifth of all X-EDA-ID patients [12] and is usually reported as inflammatory bowel disease (IBD), atypical colitis, or Behcet's disease [6, 11, 13]. The onset of inflammatory colitis occurs early in childhood and often causes failure to thrive [2, 5–7, 9, 11–13]. The age of onset of colitis in X-EDA-ID is earlier than that of Crohn's disease, ulcerative colitis, or chronic granulomatous disease [14]. Histological examination reveals active colitis with abundant neutrophilic infiltration, and the colitis usually improves with corticosteroids but not with antimicrobial agents [6, 11]. Susceptibility to colitis remains after hematopoietic stem cell transplantation [6, 9].

Recently, Nenci et al. demonstrated that mice lacking NEMO in intestinal epithelial cells developed spontaneous severe colitis [15]. However, an additional lack of tumor necrosis factor (TNF) receptor-1 in these mice inhibited intestinal inflammation. These interesting findings suggest that TNFα plays a role in the progression of NEMO colitis and that TNF blockade therapy would be a promising treatment.

We describe here an X-EDA-ID boy suffering from severe intractable colitis who improved dramatically following treatment with a chimeric anti-TNFα monoclonal antibody, infliximab. Infliximab administration reduced all symptoms relating to inflammatory colitis, not only frequent diarrhea and severe abdominal pain, but also inflammatory findings by colonoscopy. These effects have lasted for more than 2 years with regular administrations of infliximab.

Methods

Cell Preparation and Culture

Peripheral blood mononuclear cells (PBMCs) were isolated from peripheral blood from our X-EDA-ID patient and his mother using Ficoll-Paque gradient centrifugation. PBMCs were suspended in RPMI 1640 medium (Sigma-Aldrich, USA) and non-adherent cells were used to obtain stimulated T cells. Adherent cells were cultured for 10 days with 500 U/mL granulocyte-macrophage colony-stimulating factor (GM-CSF) (Peprotech, USA) to induce monocyte proliferation. T cells were stimulated for 48 h with 1-μg/mL phytohemaggulutinin (PHA) (Seikagaku Kogyo, Japan) and then for 8 days with 10-U/mL recombinant human interleukin (IL)-2 (Genzyme Techne, USA).

Cytokine Production Assay

PBMCs from our patient and healthy volunteers were incubated with LPS (1 μg/mL) (Sigma-Aldrich) at a concentration of 1×10^6 cells/mL at 37°C for 24 h. The concentration of TNFα in supernatant was measured using human BD OptEIA enzyme-linked immunosorbent assay kits (Becton-Dickinson, USA).

Mutation Analysis and Reversion Analysis

Genomic DNA from our patient and his mother was extracted from PBMCs, stimulated T cells, and stimulated monocytes using Puregene DNA purification kit (Gentra/Qiagen, USA); total RNA was extracted using TRIzol, according to the manufacturer's instructions (Invitrogen, USA). Complementary DNA (cDNA) was synthesized from total RNA with TaKaRa RNA PCR™ Kit (AMV) (Takara, Japan). Polymerase chain reaction (PCR) of genomic DNA and cDNA was performed using TaKaRa LA Taq (TaKaRa) with primers to amplify between exon 2 and exon 4 in the *IKBKG* gene. PCR primers were as follows: c1F, 5′-GCGCTCCTGAGACCCTCCAG-3′; c2R, 5′-GAGGAGAAGGAGTTCCTCAT-3′; G3F, 5′-CCCAGCTCCCCTCCACTGTC-3′; G4R, 5′-AACCCTG GAAGGGGTCTCCGGAG-3′. Genomic DNA was denatured at 94°C for 3 min, followed by 35 cycles of denaturation at 94°C for 30 s, annealing at 64°C for 30 s, and elongation at 68°C for 2 min 30 s, and a final extension for 7 min at 72°C using G3F and G4R primers. cDNA was denatured at 94°C for 1 min, followed by 35 cycles of denaturation at 94°C for 30 s, annealing and elongation at 68°C for 1 min, and a final extension for 5 min at 68°C using c1F and c2R primers. After gel electrophoresis and visualization, targeted bands were extracted and sequenced using ABI Big-Dye Terminator (Applied Biosystems, USA).

To analyze the reversion of mutation, we used our X-EDA-ID patient's PBMCs and stimulated cells. Mononuclear cells sorted with FACSVANTAGE (Becton-Dickinson) were used only at analysis after 12 months of infliximab treatment. PCR products were subcloned using a TOPO

TA cloning kit (Invitrogen) and sequenced as described above.

Reporter Assay for Detecting a Mutant NEMO Function: NEMO-NF-κB Luciferase Reporter Assay

NEMO cDNAs from a healthy volunteer and our patient were subcloned into the p3xFLAG-CMV14 vector (Sigma), respectively. NEMO null rat fibroblast cells (kindly provided by Dr. S. Yamaoka) were plated at a density of 3×10^4 cells/well in a 24-well culture dish and were transfected with 200 ng of plasmid, containing 40 ng of NF-κB reporter plasmid (pNF-κB-Luc; BD Biosciences Clontech, USA), 2 ng of a *NEMO* mutant expression construct, 148 ng internal control for normalization of transfection efficiency (pRL-TK; Toyo Ink, Japan), and the corresponding mock vector, using the FuGENE® HD Transfection Reagent (TOYO-B-Net, Japan) according to the manufacturer's protocol. At 12 h after transfection, the cells were stimulated with 15 ng/mL LPS for 4 h and the NF-κB activity was measured using the PicaGene® Dual SeaPansy assay kit (TOYO-B-NET) according to the manufacturer's protocol. Experiments were performed in triplicate and firefly luciferase activity was normalized to Renilla luciferase activity.

Vβ and Vα Analysis of T Cells

T cell receptor (TCR) β and α chain variable region (Vβ and Vα) repertoires were analyzed by a reverse transcription polymerase chain reaction (RT-PCR) method as described [16]. Briefly, each Vβ fragment (from Vβ1 to Vβ20) or Vα fragment (from Vα1 to Vα18, Vα21, and Vα24) was prepared from a series of HBVT/HBVP or HAVT/HAVP plasmids originating from thymus or peripheral T cells [17] and was dotted on filters. PCR products obtained from the patient by RT-PCR were labeled by α-^{32}P-dCTP and hybridized to the filters. Using densitometry, a semiquantitative assessment of V gene usage was made from the amounts of hybridized products.

Flow Cytometry

Peripheral blood samples were analyzed by three-color flow cytometry. Cells were stained with monoclonal antibodies to the following cell surface markers: CD3, CD4, CD8, CD19 (Becton-Dickinson), and CD14 (eBioscience, USA). Flow cytometry analysis of intracellular NEMO protein was performed as described previously [18]. Flow cytometric data from the stained cells were collected by FACScalibur and analyzed with CellQuest software (Becton-Dickinson).

Intracellular Cytokine Staining

Whole blood samples from our X-EDA-ID patient and healthy donors were stimulated with 1-μg/mL ionomycin (Sigma-Aldrich) and 25-ng/mL phorbol 12-myristate 13-acetate (PMA) (Sigma-Aldrich) in the presence of 10-μg/mL brefeldin A (Sigma-Aldrich) for 4 h. Cultured cells were stained with monoclonal antibodies against CD4 and CD8 for 30 min at room temperature. Stained cells were fixed and permeabilized with BD Lysing solution (Becton-Dickinson) and incubated with anti-TNFα monoclonal antibody or IgG1 isotypic control (Becton-Dickinson). Cells were analyzed by flow cytometry as described above. Analysis of intracellular TNFα in CD14+ cells was performed after stimulation with LPS (1 μg/mL) at 37°C for 4 h.

Endoscopy and Immunohistochemical Staining

Endoscopy was performed with the consent of legal guardians. Colon biopsies were obtained at regions of visual abnormalities. Formalin-fixed paraffin-embedded tissues blocks were cut into 2-μm sections and stained with hematoxylin and eosin. Subsequently, immunohistochemical analysis using the following primary antibodies with optimized experimental protocols was performed: CD3ε (DAKO, Denmark, rabbit, polyclonal, diluted 1:100, incubated for 24 h at 4°C after microwave heat-induced antigen retrieval for 40 min in pH 6.0 citrate buffer), CD79a (DAKO, mouse, monoclonal, 1:100, microwave for 40 min, pH 6.0), CD68 (DAKO, mouse, monoclonal, 1:50, proteinase K (DAKO) for 10 min at room temperature), CD4 (Novocastra, USA, 1:100, microwave for 40 min, pH 9.0 (NICHIREI BIOSCIENCES, Japan)), CD8 (DAKO, mouse, monoclonal, 1:100, microwave for 40 min, pH 9.0), and TNFα (Santa Cruz Biotechnology, USA, goat, polyclonal, 1:200, microwave for 40 min, pH 6.0). An Envision-HRP Detection kit (DAKO) was used for visualization, except for anti-TNFα, which was visualized using donkey biotin conjugated anti-goat secondary antibody (Jackson ImmunoResearch Laboratories, USA) and LASB2-System/HRP kit (DAKO).

Infliximab Treatment

Infliximab treatment for our X-EDA-ID patient was approved by the medical ethics committee of the University of Miyazaki. We obtained written consent concerning treatment from both the patient and his guardian. Before initiating infliximab, we confirmed that he had no severe infection including tuberculosis according to laboratory data, mycobacterium culture test, skin tuberculin test, and chest computed tomography. Cardiac dysfunction was excluded by echocardiography and electrocardiogram.

Infliximab was given intravenously over 2 h at a dose of 5 mg/kg on 0, 2, and 6 weeks, with follow-up treatments every 7–8 weeks depending on clinical symptoms. The patient was monitored regularly throughout the infliximab treatment.

Results

Case

The patient was born to unrelated Japanese parents after an uncomplicated pregnancy of 41 weeks. There was no history of any first-degree relative diagnosed with incontinentia pigmenti. On the first day after birth, he presented high fever with a markedly increased white blood cell count ($40\times10^3/\mu L$) and was treated successfully with antibiotics. He has had a history of recurrent, severe infections including varicella at 3 months of age, penicillin-resistant *Streptococcus pneumoniae* meningitis at 6 months of age, and zoster at 8 months of age. Persistent diarrhea was also observed.

He was introduced to our hospital at 8 months of age for examination of his immunological status. On admission, he showed a marked increase in both white blood cells ($31.9\times10^3/\mu L$) and platelets ($872\times10^3/\mu L$). Peripheral blood T cell count was decreased (CD3-positive cells, 25.8%), and B cell count was highly increased (CD20-positive cells,: 69.2%). PHA induced a normal proliferation response of T cells, and concentrations of immunoglobulins were within the normal range except IgD (less than 0.2 mg/dL). Natural killer cell activity was markedly impaired. Superoxide-generating ability from neutrophils was intact. LPS-induced TNFα production from patient's PBMC was impaired (Fig. 1a). Interferon (IFN) γ-producing lymphocytes were also reduced apparently at 8 months of age (Table I). All the genes involving in the IL-12 signal pathway, including *IL12RB1*, *IL12RB2*, *JAK2*, and *STAT4* were sequenced, but no mutations were found (data not shown). Surprisingly, both IFNγ-producing T cells and natural killer cells had expanded significantly by 11 months of age (Table I). In addition, we observed that he had ectodermal dysplasia including anhidrosis and conical teeth (Supplementary Fig. 1). A skin biopsy revealed the absence of eccrine sweat glands. When he was 3 years old, a G505C (A169P) missense mutation in his *IKBKG* gene was confirmed and diagnosed as X-EDA-ID. His mother was a carrier. An expression of mutant NEMO protein was not markedly

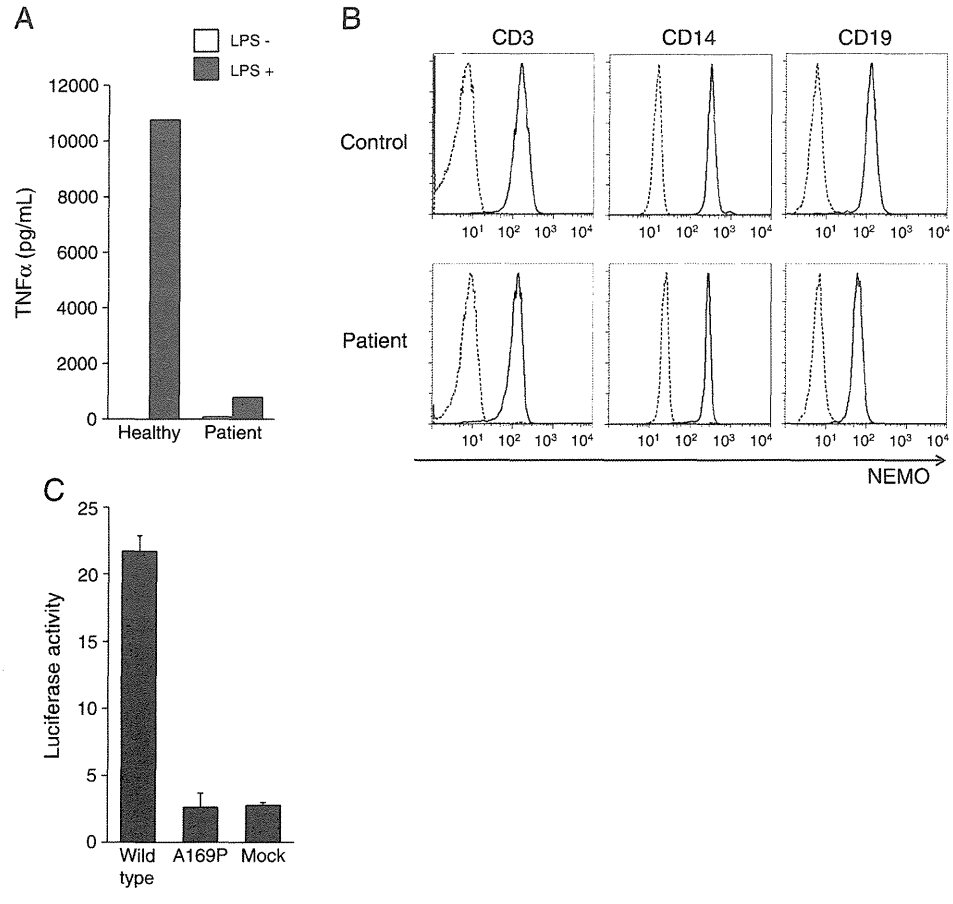

Fig. 1 Analysis of mutant NEMO protein. **a** Reduced production of TNFα from LPS-stimulated PBMCs. PBMCs from our patient and healthy volunteer were stimulated with LPS (1 μg/mL). **b** Analysis of NEMO protein expression using flow cytometry. Intracellular NEMO protein in PBMCs from the patient was not reduced markedly. **c** The result of NEMO-NF-κB luciferase reporter assay. The activity of mutant NEMO in the patient was almost defective. Mock vectors and wild-type NEMO were used as controls. *Error bars* indicate SD

Table I Proportion of IFNγ-expressing T and NK cells in the patient

Age	$IFN\gamma^+/IL\text{-}4^-$		
	CD4 (%)	CD8 (%)	CD56 (%)
8 months	1.14	8.83	2.00
11 months	3.18	70.40	66.29
3 years 11 months	11.89	65.48	82.79
Healthy control	15	60–80	80–90

reduced by flow cytometer (Fig. 1b), but the activity of mutant NEMO was almost defective which was confirmed by a mutant NEMO-NF-κB luciferase reporter assay (Fig. 1c). He has been prescribed prophylactic cotrimoxazole before and after the diagnosis.

He presented with chest pain, erythema, polyarthritis, continuous high fever refractory to antibiotics, and marked elevation of C-reactive protein (7.4 mg/dL) at 4 years of age. Autoantibodies such as anti-centromere antibody were detected transiently. Chest computed tomography revealed multiple nodular shadows resembling bronchiolitis obliterans organizing pneumonia. The repertoire of T cell receptor showed high expression of limited Vβ subsets (Supplementary Fig. 2). Combination therapy using corticosteroids, cyclosporine A, and methotrexate was effective and was continued to control his symptoms.

Severe abdominal pain and intractable frequent diarrhea recurred when the corticosteroid dose was reduced, and he presented perianal fistula at 8 years of age. A mild elevation was observed in both erythrocyte sedimentation rate and C-reactive protein under the preceding immunosuppressive treatments (Table II). No significant pathogen was detected by stool culture and the use of antibiotics and antifungal drugs resulted in no improvement in clinical symptoms.

Endoscopic and Microscopic Findings of the Colon

Colonic endoscopy revealed many polyp-like lesions with mucosal redness and edema at the sigmoid/descending junction (Fig. 2). A longitudinal ulcerative lesion found in the sigmoid colon was suggestive of Crohn's disease. Passing the endoscope beyond these obstructive clusters of polyps was difficult; therefore, we could not observe the upper part of the colon. Neither stenosis nor ulcer formation was observed by intestinal radiocontrast analysis.

Histopathological examination of the colonic biopsied specimens showed diffuse lymphoplasmacytic infiltration, superficial edema, and hyperemia in lamina propria. Foamy cells and some eosinophils were also seen (Fig. 3a, b). No definite neutrophilic infiltration, crypt abscesses, or granulomatous lesions were observed. Cultures from biopsied specimens yielded neither bacterial nor fungal growth.

Immunohistochemical staining revealed predominant infiltration of CD79a-positive, plasma cells in the lamina propria. Infiltration of CD68-positive macrophages and CD3-positive T cells was also observed (Fig. 3c–g).

Detection of TNFα-Producing Cells in the Lamina Propria and Peripheral Blood

To investigate the possibility that TNFα blockade therapy can ameliorate inflammatory colitis as well as NEMO-deficient mice as suggested by previous analysis [15], we analyzed TNFα-producing mononuclear cells in the lamina propria in the colon of our patient. Immunohistochemical staining showed abundant TNFα in infiltrated mononuclear cells in the lamina propria (Fig. 3h) which would be associated with progression of inflammatory colitis.

We also analyzed TNFα-producing T cells and monocytes in the peripheral blood (Fig. 4a). The majority (72.49%) of CD4-positive T cells in our patient expressed intracellular TNFα, while 40% to 70% of CD4-positive T cells expressed TNFα in adults with IBD in our study. Forty-eight percent of CD8-positive T cells in our patient expressed TNFα. CD14-positive monocytes from our patient expressed small amounts of intracellular TNFα after LPS stimulation, while similarly treated CD14-positive cells from healthy subjects expressed abundant TNFα (Fig. 4b).

Reversion Analysis

Nishikomori et al. reported that in an X-EDA-ID patient, the mutation had been reverted to the normal state in IFNγ-

Table II Laboratory data on admission (8 years old)

WBC	13,600/μL	CD3	76.2%	IgG	790 mg/dL
Neutrophils	10,200/μL	CD4	22.2%	IgA	666 mg/dL
Lymphocytes	1,632/μL	CD8	58.3%	IgM	71 mg/dL
Monocytes	952/μL	CD19	4.8%	IgD	<0.6 mg/dL
Hemoglobin	12.0 g/dL	CD20	3.8%	C3	134 mg/dL
Platelets	84.7×10^4/μL	CD16	0.5%	C4	46 mg/dL
		CD56	33.6%	CH50	56 U/mL
		HLA-DR	26.5%	ESR	43 mm/h

WBC white blood cell, *CH50* total complement activity, *ESR* erythrocyte sedimentation rate

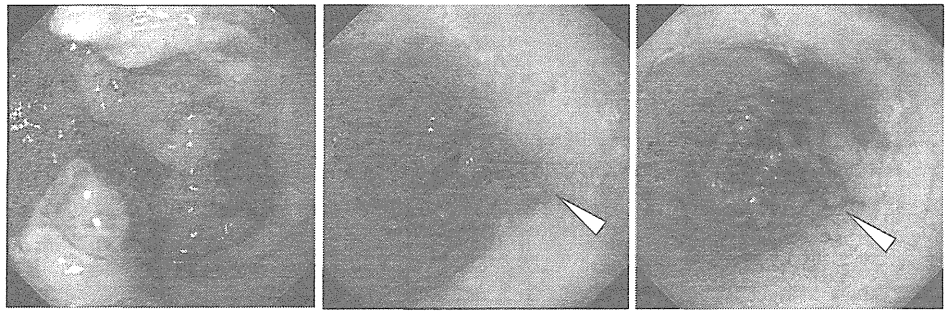

Fig. 2 Findings of colonoscopy performed before initial treatment with infliximab. Colonoscopy revealed polyp-like lesions with mucosal redness and edema at the sigmoid/descending junction (*left panel*). A longitudinal ulcer (*arrowhead*) was found in the sigmoid colon (*center panel*). Same segment as in the *center panel* after indigo carmine dye (*right panel*)

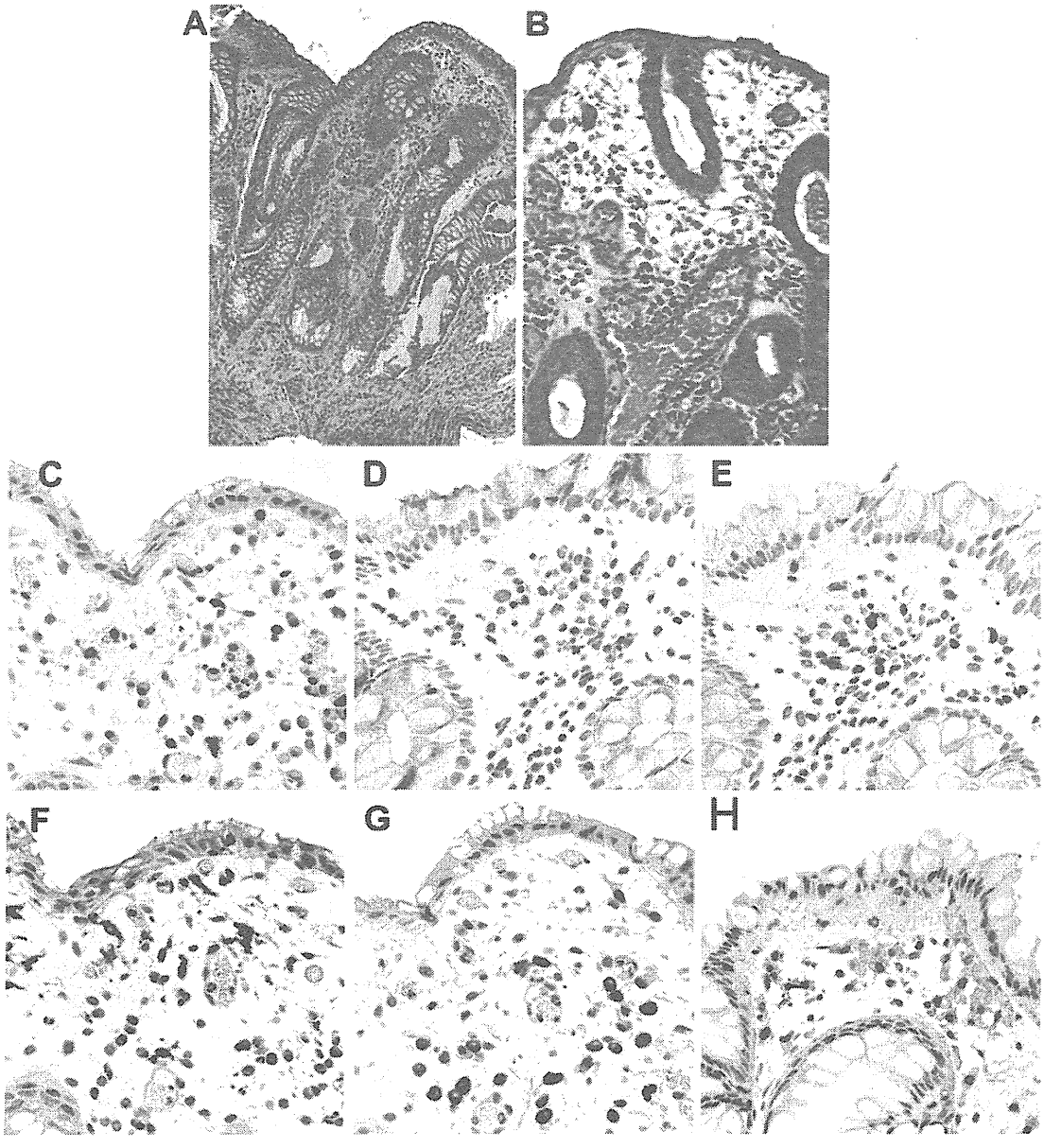

Fig. 3 Microscopic findings of affected colonic specimens. **a**, **b** Hematoxylin and eosin staining. **a** and **b** are low-power field and high-power field views, respectively. **c**–**h** Staining profiles of cellular surface antigens: **c** CD3ε, **d** CD4, **e** CD8, **f** CD68, and **g** CD79a. **h** Staining with anti-human TNFα antibody

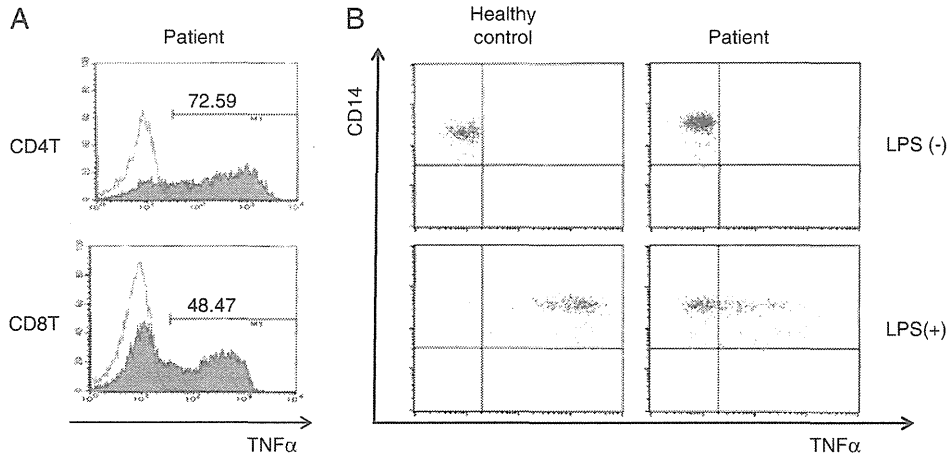

Fig. 4 Analysis of TNFα-producing mononuclear cells in peripheral blood. **a** TNFα-expressing T cells increased markedly before infliximab treatment. PBMCs were stimulated with ionomycin and PMA for 4 h in the presence of brefeldin A then stained for intracellular TNFα. For FACS analysis, gates were set on lymphocytes according to forward and side scatter properties. Representative histograms of TNFα expression in stimulated (*solid histograms*) or unstimulated (*black line histograms*) T cells. The proportion of TNFα-positive CD4-positive T cells in adult IBD patients is 40–70%. **b** The percentage of TNFα-positive monocytes was examined. Cells from our patient and healthy volunteer were incubated with or without LPS for 4 h in the presence of brefeldin A. Monocytes were identified by CD14. Approximately 50% of stimulated monocytes produced a small amount of TNFα

expressing T cells [18]. Our patient showed expansion of IFNγ-expressing T cells during infancy and an increase in TNFα-producing T cells at that time. We hypothesized that the A169P mutation in the *IKBKG* gene had been reverted to wild type and that the reverted T cells had expanded in our patient. Indeed, before initiating infliximab treatments, reversion mutation was detected in 23/67 (34%) from non-stimulated PBMCs (Table III). At 24 months after the initiation, reversion mutation was detected in both messenger RNA (mRNA) and genomic DNA from lymphocytes stimulated with PHA and IL-2 for 10 days, whereas only mutated mRNA was identified from non-stimulated lymphocytes (Fig. 5). Reverted mRNA was observed in CD3-positive T cells. Sex chromosome analysis with fluorescent in situ hybridization revealed no maternal cells and therefore graft-versus-host disease secondary to maternal–fetal transfusion was unlikely. These findings suggest that reverted T cells activated NF-κB in response to growth signals and had a growth advantage over mutant cells.

Table III Frequency of reverted clones before and after initiation of infliximab treatments

	Before	After 12 months	After 24 months
PBMCs	23/67 (34%)	nd	2/6 (33%)[a]
CD3	nd	3/16 (19%)	nd
CD14	nd	0/19 (0%)	nd
CD19	nd	0/47 (0%)	nd

nd not done

[a] A result using stimulated mononuclear cells

Reverted T cells decreased with repeated administrations of anti-TNFα monoclonal antibody. In contrast, CD14-positive monocytes and GM-CSF-induced monocyte-derived dendritic cells had no reversion (Table III).

Anti-TNFα Treatment Improved NEMO Colitis

We initially treated NEMO colitis with high dose corticosteroid therapy (2 mg/kg prednisolone, daily) (Fig. 6). However, steroid therapy did not improve clinical symptoms and resulted in compression fracture in the thoracic spine from corticosteroid-induced osteoporosis.

The increase in TNFα-producing T cells suggested the possibility that TNFα blockade therapy would be an effective treatment for the intractable NEMO colitis. After confirming the absence of severe bacterial or mycobacterial infection, we initiated administration of the chimeric anti-TNFα monoclonal antibody, infliximab, to our patient.

Soon after the first infusion of infliximab, abdominal pain disappeared and his appetite recovered. Frequency of diarrhea decreased as administrations of infliximab were repeated (Fig. 6). Colonoscopy after his third administration showed mild improvement of both mucosal redness and edema (Fig. 7a). These mucosal inflammatory findings had almost disappeared after 1-year treatment with infliximab, although polyp-like lesions remained (Fig. 7b).

The proportion of TNFα-producing cells in CD4-positive and CD8-positive T cells markedly decreased by his third infliximab infusion (from 72.6% to 26.7% in CD4-positive T cells and from 48.5% to 23.1% in CD8-positive T cells), and reduction of TNFα-producing cells was

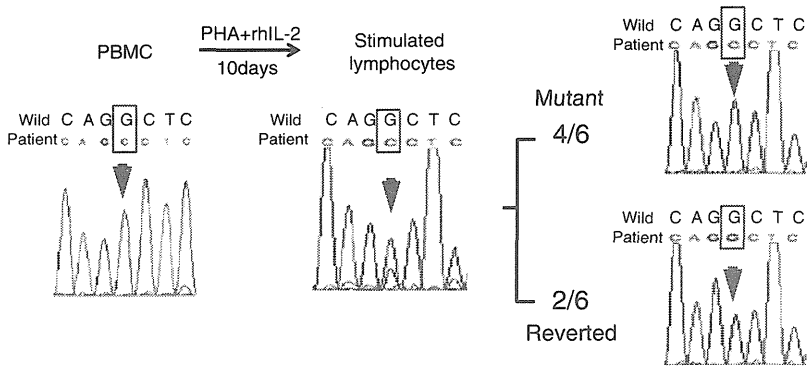

Fig. 5 Reversion analysis of cDNA of gene encoding NEMO isolated from mononuloclear cells after 24 months of infliximab treatment. PBMC was obtained from our patient and incubated with PHA and IL-2 for 10 days. Direct sequence for mRNA encoding NEMO was performed using PBMC and the stimulated mononuclear cells. Before stimulation, no reverted mononuclear cells were detected. After PHA and IL-2 stimulation, reverted mononuclear cells apparently increased. Subcloning of cDNA from stimulated cells showed that two of six cells had reversion of mutation in the gene

associated with improvement of clinical symptoms (Fig. 6). Administration of cyclosporine A was discontinued by the eighth infliximab treatment, and corticosteroid was reduced and then discontinued by the tenth infliximab infusion.

Our patient had one serious adverse event, pneumonia, after his fourth administration of infliximab. *Campylobacter jejuni* was isolated from his blood culture at that time. He was successfully treated with antibiotics and infliximab administration was resumed after confirming resolution of pneumonia. He has been treated safely for more than 2 years with regular administrations of infliximab (once every 7–8 weeks). Neither mycobacterial infections nor severe infusion reactions have been observed.

Discussion

Our patient showed immunodeficiency with very low IFNγ-production during his younger years as shown in Table I and suffered from many opportunistic infections (Zoster virus infection, penicillin-resistant *Streptococcus pneumoniae* meningitis, and other undetermined infections). A novel missense mutation, A169P, in the first coiled-coil domain resulted in defective NEMO function (Fig. 1) and was responsible for recurrent severe infections. However, he later suffered from autoimmune diseases at 4 years of age (bronchiolitis obliterans organizing pneumonia, severe arthritis, and vasculitis) and severe chronic inflammatory colitis at 8 years. Based on the facts that, in the mice model, TNFα played a major role in the pathogenesis of NEMO colitis [15], and that, in our patient, TNFα-producing mononuclear cells in the peripheral blood were markedly increased (Fig. 4a), infliximab was employed for the patient's treatment. This treatment led to improvement in his symptoms and colonoscopic findings for 2 years.

Increases in TNFα-producing cells similar to that seen in other IBD [19] were detected (Fig. 4). We confirmed G/C

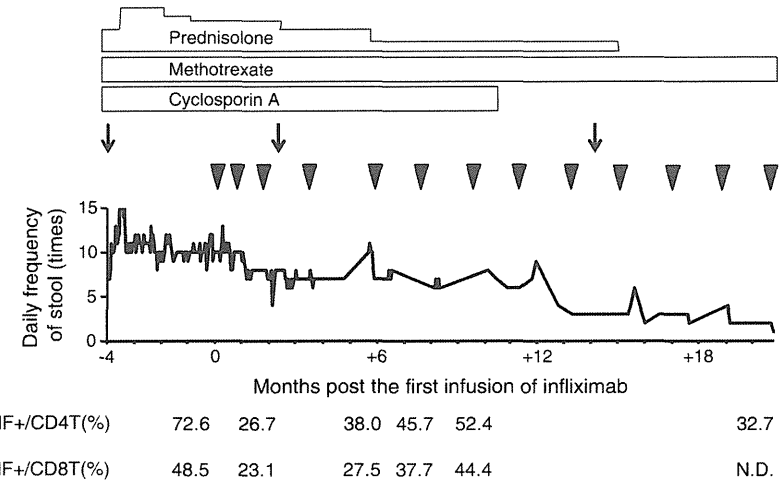

TNF+/CD4T(%)	72.6	26.7	38.0	45.7	52.4	32.7
TNF+/CD8T(%)	48.5	23.1	27.5	37.7	44.4	N.D.

Fig. 6 Clinical course of NEMO colitis after infliximab treatment in our patient. Colonoscopy (*arrows*), administrations of infliximab (*arrowheads*), and other immunosuppressive drugs (*bars*) are indicated. Daily frequency of stools (times) is graphed at the *center*. Changes in the proportion of TNFα-producing T cells in CD4-positive and CD8-positive cells are also indicated at the *bottom*

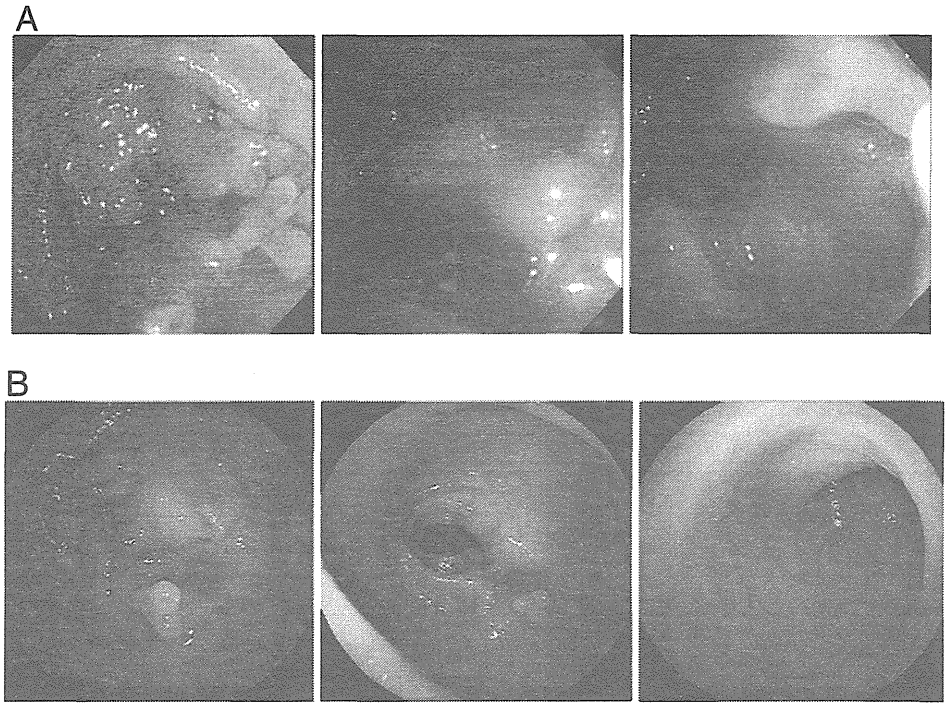

Fig. 7 Findings of colonoscopy after infliximab treatment. **a** Colonoscopy performed after the third infliximab treatment. Mild improvement was observed. Both mucosal redness and edema decreased. However, polyp-like lesions remained. At this point, the patient showed neither abdominal pain nor watery diarrhea. **b** Colonoscopy after 1-year treatment. Almost no mucosal redness or edema. A clear vascular pattern was also observed. Inflammatory polyps could still be found

reversion in T cells after co-stimulation with PHA and IL-2 before and even after infliximab therapy (Table III and Fig. 5). Reversion mosaicism has been reported in primary immunodeficiencies such as X-linked severe combined immunodeficiency [20, 21], adenosine deaminase deficiency [22], *RAG1* deficiency [23], and Wiskott–Aldrich syndrome [24]. Most of these patients reduced the frequency of severe infections and showed survival for longer periods. Our patient also had very few episodes of severe infection after expansion of IFNγ-producing peripheral blood mononuclear cells, contrary to increased susceptibility to diverse pathogens in X-EDA-ID [5, 25]. However, none of the patients with reversion mosaicism involving reverted T cells developed IBD other than X-EDA-ID. Our patient and patients with Omenn's syndrome [21, 23] developed systemic inflammatory conditions and exhibited a restricted TCR repertoire. In our patient, oligoclonal expansion of reverted T cells caused impairment of immune regulation.

According to the report by Nenci et al. in a murine model of intestinal epithelium-specific NEMO deficiency, intestinal epithelial cells exhibit increased sensitivity to TNFα-induced apoptosis and cause disruption of the epithelial barrier if mucosal immune cells have normal immune functions and produce proinflammatory cytokines [15]. They also showed that an additional TNF receptor-1 knockout ameliorated this intestinal inflammation [15]. The pathogenesis of severe colitis in the mouse model seems to be similar to that of our patient. Specifically, NEMO-deficient intestinal epithelium was damaged by TNFα produced from both T cells and macrophages in the lamina propria (shown in Fig. 3c–e, h), and anti-TNFα antibody suppressed progression of intestinal inflammation. Although reversion in peripheral blood monocytes was not confirmed after culture with GM-CSF and analysis of TNFα expression after LPS stimulation, submucosal and peripheral macrophages produced a fair amount of TNFα detectable by immunohistochemistry and flow cytometry (Figs. 3 and 4). Production of TNFα from lamina propria macrophages may be augmented by IFNγ released from reverted T cells.

In addition to the amelioration of clinical symptoms and colonic mucosal inflammation, in our patient, TNF blockade therapy restored his dry skin with thick epidermis to moderately moist skin of normal thickness. Nenci et al. described in another paper using the epidermis-specific NEMO-deficient mice that mice showed severe skin inflammation with thick epidermis and predominant infiltration of inflammatory cells and showed further that an additional knockout of TNFR1 suppressed the inflammatory condition [26]. We postulate that TNFα is also a key cytokine in the pathogenesis of inflammation in diverse epithelial tissues and that infliximab treatment suppresses the TNFα-mediated inflammatory response by inducing apoptosis of TNFα-producing cells [27]. In fact, the patient's peripheral blood TNFα-producing cells reduced along with the improvement of clinical symptoms, and this reduction provided an available marker to assess inflammatory status. Reverted cells in peripheral blood also decreased after repeated anti-TNFα antibody administrations. Unfortunately, we could not obtain consent for re-biopsy so we could not

confirm a vulnerability for apoptosis of intestinal epithelium and lamina propria after the treatment.

Since patients with X-EDA-ID were well known to have increased susceptibility to mycobacterium, and in addition, anti-TNFα monoclonal antibody indeed caused infection-related deaths in a few patients with inflammatory colitis associated with primary immunodeficiencies [28–30], the side effects of anti-TNFα monoclonal antibody treatment should be paid attention to, especially, mycobacterial infections. Before infliximab treatment, we confirmed the absence of active mycobacterial infections by culture tests for mycobacterium including atypical mycobacteria, laboratory examinations, and chest radiographs. He also has no history of Bacillus Calmette-Guérin immunization. Although the patient experienced bacterial pneumonia after his third infliximab infusion, he has not suffered from severe infections for several years. This may be because of the patient's mosaicism of mutated and reverted cells. The risks concerning severe infections and oncogenic effects [31–33] should be considered before employing infliximab for NEMO colitis.

Conclusion

Reversion of mutation in T cells contributes to the pathogenesis of mucosal immunity in NEMO-deficient patients. Moreover, treatment with anti-TNFα monoclonal antibody therapy can improve the symptoms of the disease by both preventing exposure of the mucosa to TNFα and reducing the number of T cells carrying the reverted gene. Anti-TNFα monoclonal antibody therapy provides a promising treatment for intractable NEMO colitis.

Acknowledgments We profoundly thank for Dr. Kazuko Uno of the Louis-Pasteur Medical Research Center in Japan for support of our experiments and Dr. Maiko Kai and Dr. Naoki Karasawa1 for their warm care of patients. This study was supported by a Grant-in-Aid for Scientific Research from the Ministry of Education, Culture, Sports, Science and Technology, Japan.

Conflict of Interests The authors declare no competing financial interests.

References

1. Zonana J, Elder M, Schneider L, et al. A novel X-linked disorder of immune deficiency and hypohidrotic ectodermal dysplasia is allelic to incontinentia pigmenti and due to mutations in IKK-gamma (NEMO). Am J Hum Genet. 2000;67:1555–62.
2. Döffinger R, Smahi A, Bessia C, et al. X-linked anhidrotic ectodermal dysplasia with immunodeficiency is caused by impaired NF-kappaB signaling. Nat Genet. 2001;27:277–85.
3. Jain A, Ma CA, Liu S, et al. Specific missense mutations in NEMO result in hyper-IgM syndrome with hypohydrotic ectodermal dysplasia. Nat Immunol. 2001;2:223–8.
4. Orange JS, Brodeur SR, Jain A, et al. Deficient natural killer cell cytotoxicity in patients with IKK-gamma/NEMO mutations. J Clin Invest. 2002;109:1501–9.
5. Orange JS, Jain A, Ballas ZK, et al. The presentation and natural history of immunodeficiency caused by nuclear factor kappaB essential modulator mutation. J Allergy Clin Immunol. 2004;113:725–33.
6. Pai S, Levy O, Jabara H, et al. Allogeneic transplantation successfully corrects immune defects, but not susceptibility to colitis, in a patient with nuclear factor-kappaB essential modulator deficiency. J Allergy Clin Immunol. 2008;122:1113–1118.e1111.
7. Tono C, Takahashi Y, Terui K, et al. Correction of immunodeficiency associated with NEMO mutation by umbilical cord blood transplantation using a reduced-intensity conditioning regimen. Bone Marrow Transplant. 2007;39:801–4.
8. Mancini AJ, Lawley LP, Uzel G. X-linked ectodermal dysplasia with immunodeficiency caused by NEMO mutation: early recognition and diagnosis. Arch Dermatol. 2008;144:342–6.
9. Fish J, Duerst R, Gelfand E, et al. Challenges in the use of allogeneic hematopoietic SCT for ectodermal dysplasia with immune deficiency. Bone Marrow Transplant. 2009;43:217–21.
10. Permaul P, Narla A, Hornick J, et al. Allogeneic hematopoietic stem cell transplantation for X-linked ectodermal dysplasia and immunodeficiency: case report and review of outcomes. Immunol Res. 2009;44:89–98.
11. Cheng L, Kanwar B, Tcheurekdjian H, et al. Persistent systemic inflammation and atypical enterocolitis in patients with NEMO syndrome. Clin Immunol. 2009;132:124–31.
12. Hanson E, Monaco-Shawver L, Solt L, et al. Hypomorphic nuclear factor-kappaB essential modulator mutation database and reconstitution system identifies phenotypic and immunologic diversity. J Allergy Clin Immunol. 2008;122:1169–1177.e1116.
13. Takada H, Nomura A, Ishimura M, et al. NEMO mutation as a cause of familial occurrence of Behçet's disease in female patients. Clin Genet. 2010;78:575–9.
14. Marks DJ, Miyagi K, Rahman FZ, et al. Inflammatory bowel disease in CGD reproduces the clinicopathological features of Crohn's disease. Am J Gastroenterol. 2009;104:117–24.
15. Nenci A, Becker C, Wullaert A, et al. Epithelial NEMO links innate immunity to chronic intestinal inflammation. Nature. 2007;446:557–61.
16. Nagano M, Kimura N, Ishii E, et al. Clonal expansion of alphabeta-T lymphocytes with inverted Jbeta1 bias in familial hemophagocytic lymphohistiocytosis. Blood. 1999;94:2374–82.
17. Kimura N, Toyonaga B, Yoshikai Y, et al. Sequences and repertoire of the human T cell receptor alpha and beta chain variable region genes in thymocytes. Eur J Immunol. 1987;17:375–83.
18. Nishikomori R, Akutagawa H, Maruyama K, et al. X-linked ectodermal dysplasia and immunodeficiency caused by reversion mosaicism of NEMO reveals a critical role for NEMO in human T-cell development and/or survival. Blood. 2004;103:4565–72.
19. Ogura Y, Imamura Y, Murakami Y, et al. Intracellular cytokine patterns of peripheral blood T cells as a useful indicator of activeness of Crohn's disease. Hiroshima J Med Sci. 2005;54:1–8.
20. Stephan V, Wahn V, Le Deist F, et al. Atypical X-linked severe combined immunodeficiency due to possible spontaneous reversion of the genetic defect in T cells. N Engl J Med. 1996;335:1563–7.
21. Wada T, Yasui M, Toma T, et al. Detection of T lymphocytes with a second-site mutation in skin lesions of atypical X-linked severe combined immunodeficiency mimicking Omenn syndrome. Blood. 2008;112:1872–5.
22. Hirschhorn R, Yang D, Puck J, et al. Spontaneous in vivo reversion to normal of an inherited mutation in a patient with adenosine deaminase deficiency. Nat Genet. 1996;13:290–5.
23. Wada T, Toma T, Okamoto H, et al. Oligoclonal expansion of T lymphocytes with multiple second-site mutations leads to